RESEARCH ARTICLE

Key Points:
- Organic carbon burial rates increased by factors of 2.5 to 6.2 for mangroves and 1.4 to 2.4 for coastal freshwater marshes in the past ~120 years
- Increasing rates represent acceleration rather than a record influenced by an artefact of the dating method or postdepositional degradation
- Acceleration has increased soil carbon stocks by 5.7–8.0 kg m^{-2} for mangroves and 4.2–4.5 kg m^{-2} for coastal freshwater marshes

Supporting Information:
- Supporting Information S1

Correspondence to:
J. L. Breithaupt,
jlbreith@mail.usf.edu

Increasing Rates of Carbon Burial in Southwest Florida Coastal Wetlands

Joshua L. Breithaupt[1] , Joseph M. Smoak[2] , Thomas S. Bianchi[3] , Derrick R. Vaughn[3,4] , Christian J. Sanders[5] , Kara R. Radabaugh[6] , Michael J. Osland[7] , Laura C. Feher[7] , James C. Lynch[8], Donald R. Cahoon[9] , Gordon H. Anderson[10] , Kevin R.T. Whelan[11] , Brad E. Rosenheim[2] , Ryan P. Moyer[6] , and Lisa G. Chambers[1]

[1]Department of Biology, University of Central Florida, Orlando, FL, USA, [2]University of South Florida, St. Petersburg, FL, USA, [3]Department of Geological Sciences, University of Florida, Gainesville, FL, USA, [4]Department of Earth, Ocean & Atmospheric Science, Now at Florida State University, Tallahassee, FL, USA, [5]National Marine Science Centre, Southern Cross University, Coffs Harbour, New South Wales, Australia, [6]Florida Fish and Wildlife Conservation Commission, Saint Petersburg, FL, USA, [7]U.S. Geological Survey, Lafayette, LA, USA, [8]U.S. National Park Service, Washington, DC, USA, [9]U.S. Geological Survey, Laurel, MD, USA, [10]U.S. Geological Survey, Gainesville, FL, USA, [11]U.S. National Park Service, Miami, FL, USA

Abstract Rates of organic carbon (OC) burial in some coastal wetlands appear to be greater in recent years than they were in the past. Possible explanations include ongoing mineralization of older OC or the influence of an unaccounted-for artifact of the methods used to measure burial rates. Alternatively, the trend may represent real acceleration in OC burial. We quantified OC burial rates of mangrove and coastal freshwater marshes in southwest Florida through a comparison of rates derived from ^{210}Pb, ^{137}Cs, and surface marker horizons. Age/depth profiles of lignin: OC were used to assess whether down-core remineralization had depleted the OC pool relative to lignin, and lignin phenols were used to quantify the variability of lignin degradation. Over the past 120 years, OC burial rates at seven sites increased by factors ranging from 1.4 to 6.2. We propose that these increases represent net acceleration. Change in relative sea-level rise is the most likely large-scale driver of acceleration, and sediment deposition from large storms can contribute to periodic increases. Mangrove sites had higher OC and lignin burial rates than marsh sites, indicating inherent differences in OC burial factors between the two habitat types. The higher OC burial rates in mangrove soils mean that their encroachment into coastal freshwater marshes has the potential to increase burial rates in those locations even more than might be expected from the acceleration trends. Regionally, these findings suggest that burial represents a substantially growing proportion of the coastal wetland carbon budget.

Plain Language Summary Coastal mangroves and marshes use photosynthesis to change carbon dioxide into plant material like leaves, wood, and roots. As these materials die over time, they do not decompose the same way they might in a dry soil environment. Instead, daily ocean tides flood the soil, removing the oxygen and allowing dead plant materials to be buried and preserved for hundreds to thousands of years or more. This "carbon burial" process is a global benefit because it means that carbon dioxide, a greenhouse gas, is stored belowground where it can no longer warm the atmosphere. Mangroves and marshes bury carbon more quickly than most other ecosystems, but little is known about how burial rates change over time. In this study, we quantify how rates of carbon burial have changed in southwest Florida coastal wetlands in the past century. We find that carbon burial is 2.5–4.5 times greater today than it was a century ago in mangroves and 1.9–2.3 times greater in marshes. We propose sea-level rise as the most likely cause of increased carbon burial. Rising seas provide the means and opportunity for wetlands to bury more carbon, but if sea level rises too quickly, these wetlands may drown.

1. Introduction

1.1. Patterns of Increasing Carbon Burial and Accretion

Blue carbon ecosystems, including coastal wetlands, have some of the highest rates of organic carbon (OC) burial in the world on a per area basis (Macreadie et al., 2019; McLeod et al., 2011). These burial rates are often calculated as multidecadal averages using activity peaks of ^{137}Cs or $^{239+240}$Pu or constant

sedimentation dating models for ^{210}Pb (Appleby & Oldfield, 1992; Baskaran et al., 2017; Corbett & Walsh, 2015; Nolte et al., 2013). Constant, linear rates of burial contribute a majority of the records used to account for global average burial rates (Chmura et al., 2003, and references therein; Breithaupt et al., 2012, and references therein; Ouyang & Lee, 2014, and references therein). These averages are a necessary part of carbon budgeting because of interest in the long-term flux of components such as productivity, respiration, and aqueous export (i.e., Bouillon et al., 2008; Troxler et al., 2013). However, reliance only on multidecadal or centennial averages may give a misleading impression of burial rates as a static or stable flux. Temporal variability of OC burial is useful for identifying, quantifying, and explaining dynamic ecosystem processes and mechanisms related to energy and nutrient cycles that have contributed to the large stocks of soil OC in blue carbon ecosystems as well as potential mechanisms for their vulnerability.

There are relatively few assessments of fine-scale temporal variability (i.e., 1–5 years) of OC burial rates in coastal wetlands (Kang & Trefry, 2013; Smoak et al., 2013; Breithaupt et al., 2014; Gonneea et al., 2019; Rogers et al., 2019). The more frequent appearance of accretion (mm year^{-1}) or mass accumulation (g m^{-2} year^{-1}) rates in the literature has contributed to several analyses noting that these rates often appear to be greater in recent years or decades than they were in the past (Breithaupt et al., 2018; Corbett et al., 2007; Jenkins, 2018; Parkinson et al., 1994; Parkinson et al., 2017). In a review of coastal wetland literature, Breithaupt et al. (2018) noted a generally negative correlation between timescale length (including subdecadal, decadal, centennial, and millennial timescales) and vertical accretion rates in places like Long Island Sound and southwest Florida (USA), the northwestern Mediterranean, and eastern Australia. Parkinson et al. (1994) found that rates of accretion measured over tens to hundreds of years were more than 2× greater than rates measured over thousands of years in Florida, Mexico, and the Caribbean. Conversely, there are other indications that sedimentation rates in recent years are lower than they were in the past. Such reversals can be attributed to anthropogenic disturbance, such as roadbuilding, alterations to regional hydrology, or more broadly, decreasing riverine supplies of suspended sediments for coastal accretion (Harmon et al., 2014; Krauss et al., 2018; Weston, 2014). For example, Breithaupt et al. (2018) found this to generally be the case for coastal Louisiana, as well as for Rookery Bay in southwest Florida.

The pattern of increasing OC burial and sediment accretion rates in recent decades can be interpreted in several ways relating to processes of sediment delivery and postdepositional degradation (Zimmerman & Canuel, 2000; Allison et al., 2007; Gonneea et al., 2019). The literal interpretation is that rates have accelerated. A second interpretation is that artifacts of the dating technique introduce a bias into the record and incorrectly report an increase in rates at the top of a core. A third hypothesis is that ongoing postdepositional mineralization of OC provides a misleading indication of increasing rates in the upper core intervals; in this scenario, high burial rates at the surface in the present day are expected to decrease over time so that the soil record in the future will no longer retain the complete stock of originally buried OC (Chaopricha & Marin-Spiotta, 2014; Marin-Spiotta et al., 2014). If this OC burial increase is real, it has numerous implications for blue carbon budgets, assessments of sink/source dynamics, and predicting the response of coastal wetlands to sea-level rise (SLR) (e.g., Shields et al., 2017).

1.2. Conservative Tracers of Organic Matter Burial

Stable mineral tracers that can be used to normalize rates of organic matter burial and ascertain time periods of addition or loss in coastal areas (Schropp et al., 1990) are scarce in regions like the Everglades of south Florida that formed atop limestone bedrock. Most mineral sediment in the region is calcareous, with the potential to dissolve in generally acidic organic coastal wetland soils (Breithaupt et al., 2017; Guan et al., 2018). Lacking a conservative, mineral tracer, we examined nutrient ratios (OC:total nitrogen [TN]), stable OC and N isotopes, and lignin content as organic indicators of diagenesis as well as noncarbonate (NC) mineral sediment as an indicator of allochthonous deposition rates.

Lignin is a biopolymer that forms up to one third of woody material in vegetation (Brown, 1969) and was used as a conservative soil organic compound because it degrades minimally in anaerobic conditions (Adair et al., 2008; Bianchi & Canuel, 2011; DeLaune & Reddy, 2008). Lignin is often used in environmental studies to differentiate organic matter inputs based on three major lignin phenol groups (cinnamyls [C], syringyls [S], and vanillyls [V]), as well as a fourth group (p-hydroxyl phenols) that is of both lignin and nonlignin origin (Jex et al., 2014). Although these groups cannot be used to distinguish between plants belonging to the same taxon (e.g., mangrove species; Thevenot et al., 2010), lignin composition does vary in vegetation depending on

tissue type (e.g., woody vs. nonwoody) and phylogeny (e.g., gymnosperms vs. angiosperms). Once in the soil, lignin may be transformed by a suite of diagenetic processes, mostly related to biological decay in the aerobic zone by fungi and bacteria (Kuzyakov, 2010; Otto & Simpson, 2006; Thevenot et al., 2010).

1.3. Research Objective

Our research objective was to determine whether previously documented increases in OC burial rates over the past century represent real acceleration or whether the increases can be attributed to postdepositional degradation of older material or to artifacts of the methods used to measure soil accumulation. Soil accumulation rates measured from ^{210}Pb and ^{137}Cs profiles were compared with nearby surface marker horizons (MHs) and used to determine OC, lignin, and NC-mineral burial rates. We utilized OC:TN age/depth profiles to look for evidence of down-core degradation and lignin: OC to assess whether down-core, postdepositional degradation had preferentially depleted the OC pool relative to total lignin. According to this interpretation, if lignin: OC remains stable over a core profile, then it is indicative of uniform rates of postdepositional degradation within the core. On its own, lignin: OC cannot indicate the occurrence or magnitude of OC mineralization, but it may indicate whether the extent of mineralization is greater for different core depths, assuming that lignin decays more slowly than the total OC pool (Henrichs, 1992). Such insights are useful for understanding whether different ages/depths of soil OC stocks are more vulnerable to remineralization than others. For a subset of cores, we also examined lignin phenols, which provide the ability to assess lignin degradation and a way to test our assumptions about the age/depth profiles of lignin: OC (Bianchi & Canuel, 2011; DeLaune & Reddy, 2008). This approach of looking at potential changes in soil OC stability provides an important nuance in the form of a time constant of preservation to blue carbon assessments that frequently focus on bulk OC stocks.

2. Methods

2.1. Study Area

Soil cores were collected from two regions of southwest Florida (Figure 1). Three cores were collected from the Rookery Bay National Estuarine Research Reserve (RB-NERR), also referred to as the Northern region: Northern Mangrove Sites 1–3 (NMg1, NMg2, and NMg3). Four cores were collected from Everglades National Park (ENP), also referred to as the Southern region: Southern Mangrove 1 (SMg1), Southern Marsh 1 (SMs1), Southern Mangrove 2 (SMg2), and Southern Marsh 2 (SMs2). Site information is available from the archived data set (https://smithsonian.figshare.com/s/211c3f093fcf7ac15939).

2.1.1. Northern Mangrove Sites

Cores from the three northern mangrove sites were collected in May 2017. The Cat's Claw Basin (NMg1) site is located adjacent to Hall Bay and Rookery Bay, both of which are protected from the Gulf of Mexico by a network of barrier islands. The closest hydrologic connection to the Gulf is approximately 5 km to the southwest. The basin mangrove forest at this site has reduced tidal influence due to the presence of an overwash berm along the western fringe of the forest, a raised road to the north, and upland habitat to the east of the forest. The soil core was collected from behind the berm, 30 m east of the bay, and 5–10 m from the nearest MH plots. The forest was dominated by mature black (*Avicennia germinans*) and red (*Rhizophora mangle*) mangroves, with occasional white (*Laguncularia racemosa*) mangroves. Stem density of trees was approximately 2,500 ha^{-1}, and average diameter at breast height (DBH) was 9.0 ± 2.9 cm. Stem density and DBH data for all three northern mangrove sites were based on data collected from trees with a DBH > 5 cm (data from Radabaugh et al., 2019).

The Blackwater Bay (NMg2) core was collected on a large mangrove island located 2 km from the mouth of the Blackwater River, approximately 3.5 km from the Gulf of Mexico and 5–10 m from the MH plots. The core was taken 25 m from the edge of the bay, near the transition between the fringe and basin forest. Average DBH of trees was 14.4 ± 10.1 cm. The forest was dominated by black and red mangroves, with a stem density of approximately 1,700 ha^{-1} (Radabaugh et al., 2019).

The Upper Faka Union Canal (NMg3) core was collected from a mangrove island located near the mouth of the Faka Union Canal, 5 km from the Gulf of Mexico and 5–10 m from the MH plots. The Faka Union canal was constructed to provide drainage for the Golden Gate Estates housing subdivision, but much of the subdivision was not developed, and the land was later converted into the Picayune Strand State Forest. The
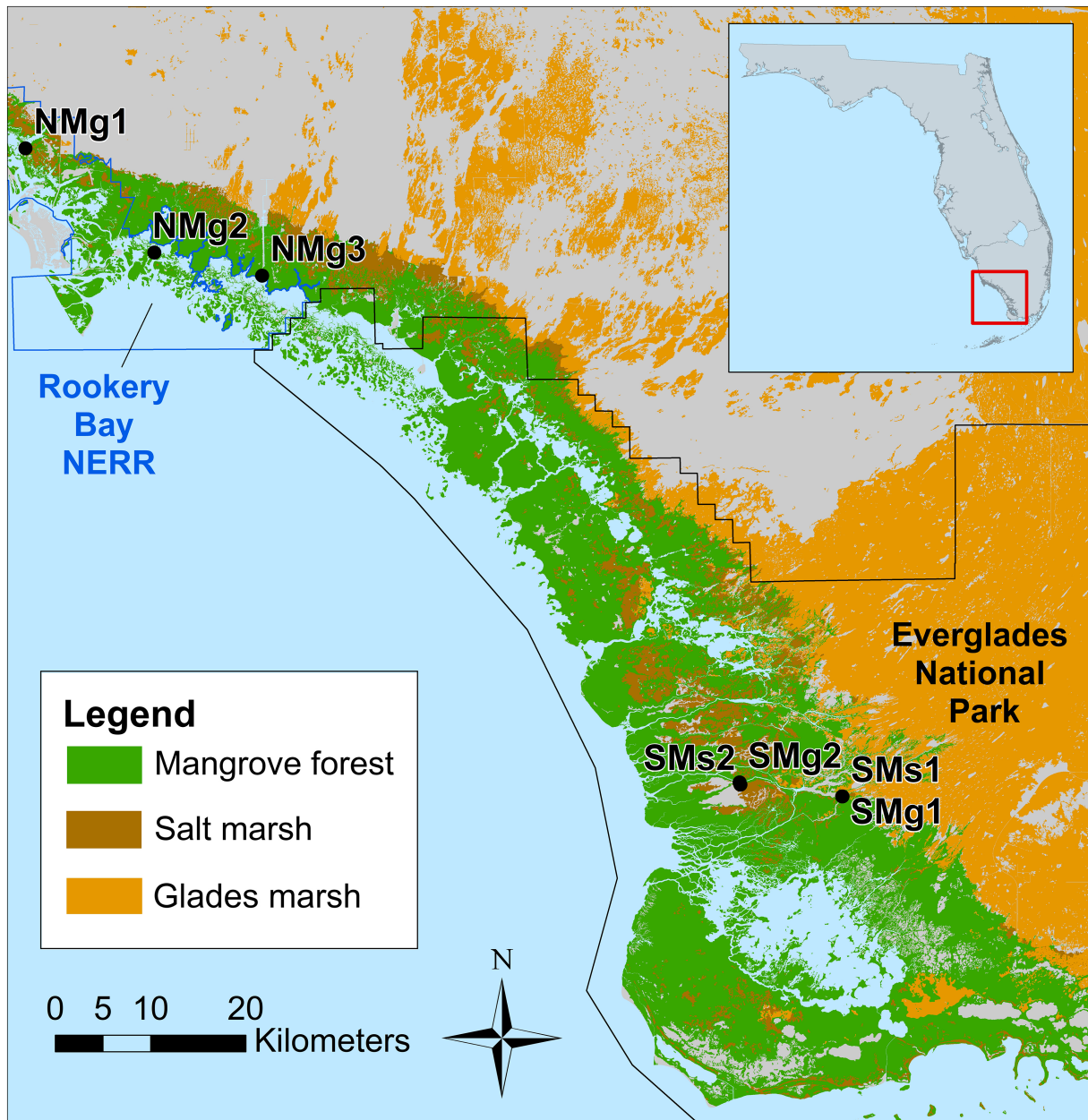
Figure 1. Sampling sites and habitat extent (FNAI and FWC, 2016) in Southwest Florida.

canal receives relatively high amounts of freshwater flow, resulting in a lower salinity in Faka Union Bay. Cores were collected 30 m from the edge of the canal near the transition between the fringe and basin forest. The forest is dominated by black and red mangroves, with scattered white mangroves. Tree stem density was approximately 2,000 ha^{-1}, and average DBH of trees was 10.9 ± 5.5 cm (Radabaugh et al., 2019).

2.1.2. Southern Mangrove and Coastal Freshwater Marsh Sites

In March 2013, four soil cores were collected in southwest ENP where riverine mangroves border interior freshwater/brackish marshes (Figure 1). These interior marshes are referred to as "Glades marshes" in the Florida Natural Areas Inventory community classification (FNAI, 2010; Figure 1). Site 1 is located on Tarpon Bay, 18 km upriver from the Gulf of Mexico, near where the Shark and Harney Rivers diverge. The mangrove core (SMg1) at this location was collected approximately 30 m from the edge of the bay. Predominant vegetation includes red and white mangroves, as well as buttonwood (*Conocarpus erectus*), that represent 71%, 8%, and 20% of stem density, respectively (Castañeda-Moya et al., 2013). Total stem density was

2,975 ha^{-1}, and average DBH was 6.2 ± 3.0 cm (Castañeda-Moya et al., 2013). The marsh core (SMs1) was collected approximately 50 m from the edge of the bay. Vegetation at this location is a mixture of sawgrass (*Cladium mariscus*) and black needle rush (*Juncus roemerianus*). Elsewhere, these sites are also referred to as SH2 (U.S. Geological Survey; Anderson et al., 2014), SRS-4 (Florida Coastal Everglades Long-Term Ecological Research program), and WSC-2 (Breithaupt et al., 2017; Breithaupt, Smoak, et al., 2019). The MH plots at this site were approximately 10 m from the radiometrically dated soil cores; the MH plots are located at the mangrove-marsh ecotone and thus do not represent either habitat type exclusively.

Site 2 is located on the southern bank of the Harney River, approximately 9 km from the Gulf of Mexico. A mangrove soil core (SMg2) was collected approximately 50 m from the river bank and 20–30 m from the mangrove MH plots. The site is composed of red, white, and black mangroves that represent 76%, 20%, and 4% of stems, respectively. Total stem density at the location of the core was 2,925 ha^{-1}, and average DBH was 8.8 ± 4.9 cm (Breithaupt, Smoak, et al., 2019). At this same location, a marsh core (SMs2) was collected approximately 300 m from the river bank and 10–20 m from the marsh MH plots. Marsh vegetation at this site is sawgrass and has been subjected to prescribed and natural wildfire events (Smith et al., 2013). The mangrove site is otherwise known as SH4 (U.S. Geological Survey; Smith et al., 2009; Smoak et al., 2013; Anderson et al., 2014) and WSC-8 (Breithaupt et al., 2017; Breithaupt et al., 2018). The marsh site is otherwise known as SH5 (U.S. Geological Survey; Jiang et al., 2013; Anderson et al., 2014).

2.2. Soil Gravimetric Characteristics

Soil cores were collected using PVC tubes (10 cm interior diameter × 50 cm length). Mechanical compaction of the soil profile during core retrieval was avoided by discarding and recollecting if soil height inside the core tube was >1 cm lower than the height of the soil surface outside the core. Soil was extruded from the core tubes and sectioned into aliquots of known volume for analysis in 1–2 cm intervals. Samples were dried at 105 °C for 24 hr for calculation of dry bulk density (DBD) based on dry mass and known aliquot volume. Samples were then combusted in a muffle furnace at the University of South Florida for 3 hr at 550 °C to determine percent loss-on-ignition as an indicator of soil organic matter (SOM). A secondary loss-on-ignition was conducted for 1 hr at 990 °C to calculate carbonate ($CaCO_3$) content (Breithaupt, Smoak, et al., 2019; Dean, 1974). Carbonate sediment may be vulnerable to dissolution in acidic pH conditions; therefore, we report NC mineral sediment (% NC-Mineral) as $1 - (\% SOM + \% CaCO_3)$ and interpret this as a conservative sediment constituent.

2.3. Chronometers: ^{210}Pb, ^{137}Cs, and Surface MHs
2.3.1. ^{210}Pb

Whereas ^{210}Pb has often been used to quantify integrated average sedimentation rates for the past century assuming a constant rate over that period, in this analysis we utilize the Constant Rate of Supply (CRS) dating model, which provided a different rate for each sectioned core interval, with ages calculated based on DBD, excess ^{210}Pb activities (dpm g^{-1}), and the relationship of the excess ^{210}Pb inventory (dpm cm^{-2}) below a given depth interval relative to that of the entire core. Sectioned intervals were dated using the CRS model for excess ^{210}Pb (Appleby & Oldfield, 1978), following the methods previously described in Smoak et al. (2013) and Breithaupt et al. (2014), Breithaupt, Smoak, et al. (2019). Briefly, ^{210}Pb and ^{226}Ra measurements were made using an intrinsic germanium detector coupled to a multichannel analyzer. Gamma counting for all cores was conducted at the University of South Florida, with each sample counted for up to 48 hr. Freeze dried, homogenized sediments were packed and sealed in gamma tubes. Activities were calculated by multiplying the counts per minute by a factor that includes the gamma ray intensity and detector efficiency. This factor was determined from standard calibrations. Identical geometry was used for all samples. The CRS dating model offers a record of temporal variability with a resolution ranging from 1 to 28 years per 1 cm depth interval (supporting information Table S1). The detection limits for ^{210}Pb and ^{226}Ra were determined for each sample using the Minimum Detectable Activity (MDA). The MDA represents the lowest activity that can be detected with a 95% confidence and is based on the counting time, background activity, sample mass, gamma ray intensity, and detector efficiency (Currie, 1988). If the activity for a given sample was less than the MDA, the activity was not statistically significant and therefore considered below detection. Activities and MDAs are provided for all ^{210}Pb and ^{226}Ra samples in the archived data set (https://doi.org/10.25573/data.9894266). The CRS dating model has an "old age bias" whereby soil age is increasingly overestimated for the oldest layers (Binford, 1990; Mackenzie et al., 2011). For this reason, we

limit our analyses of each core to depths at or above the 120 year age horizons (Table S1). Long-term average rates from the southern region mangrove cores (SMg1 and SMg2) have been previously published using site names WSC-2 and WSC-8 (Breithaupt et al., 2017; Breithaupt, Smoak, et al., 2019).

2.3.2. ^{137}Cs

When available, ^{137}Cs peaks and feldspar surface MHs were used to assess dates derived from the CRS model. Core ^{137}Cs activities can be used to identify the peak of atmospheric deposition that occurred in 1963 (Krishnaswamy et al., 1971). Because these soil cores were collected approximately 50 years after peak atmospheric ^{137}Cs deposition, this is useful for assessing the middle of the ^{210}Pb timescale. Cesium-137 activities were measured simultaneously with ^{210}Pb during gamma counting.

2.3.3. MHs

Surface accretion rates in the ^{210}Pb cores were compared with surface accretion derived from nearby surface MHs deployed by the U.S. Geological Survey at these sites. MH plots were initially deployed at NMg1 in 1993, at NMg2 and NMg3 in 1997, at SMg/Ms1 (mangrove-marsh ecotone) in 1998, and at SMg2 and SMs2 in 2006. These MH plots are associated with surface elevation table-MH (SET-MH) stations, with three or four MH plots at each SET-MH station. Approximately 3.5 kg of dry feldspar clay was deposited on the ground surface in plots of 0.5×0.5 m after removing unattached detritus (e.g., leaves and twigs). An accretion rate was determined by measuring depth to feldspar in cores collected from the MH plots over time. No physicochemical characteristics were measured from the MH cores. More information regarding the SET-MH approach is available in Cahoon, Lynch, Hensel, et al. (2002), Cahoon, Lynch, Perez, et al. (2002) and Lynch et al. (2015). More information about the SET-MH stations in the southern sites is available in Whelan et al. (2005, 2009) and Feher et al. (2019), and references for the northern sites include Lynch et al. (1989) and Cahoon and Lynch (1997). Surface elevation tables provide invaluable data about processes of vertical development in wetland soils that include accretion and erosion, in addition to expansion and contraction within the soil body. We exclude SET data from this analysis because vertical changes observed with SETs are not directly analogous to the vertical accretion measurements derived from ^{210}Pb.

2.3.3.1. Comparing ^{210}Pb and MH Accretion Rates

We compared accretion rates from approximately equivalent time frames from the ^{210}Pb CRS model and the dates of MH data collection. From the CRS model, we present the mean accretion rate $\pm$ 1 SE of the interval age calculated by propagating the uncertainties from gamma counting (Binford, 1990). For the MH data, we present the site mean linear trend of all feldspar plots, as well as the minimum and maximum trends observed from individual MH plots within each site. This ^{210}Pb uncertainty term represents the uncertainty of a single core, whereas the uncertainty of the MH represents spatial variability of the site. These differences preclude a true statistical test for difference between the two methods. Note that time period comparisons between ^{210}Pb and MH methods do not correspond exactly because dates derived from ^{210}Pb dating are dependent on soil core sectioning. For example, the bottom of depth intervals for two consecutive core sections might date from 2008 and 2004, while the MH plot might have been measured in 2006. Comparison of rates between ^{210}Pb and MH methods are further complicated by spatial variability of site topography, which contributes to variable accretion rates. A single radiometrically dated core is likely to be representative of site-scale sedimentation rates over 50–100 year timescales or longer; however, spatial variability of rates is likely to be highest over shorter 10 year timescales (Breithaupt et al., 2014). A strength of the MH method is that it integrates replicate cores from multiple subplots to ascertain the variability of sediment accretion within the footprint of a plot.

2.3.3.2. Comparing OC Burial Rates With ^{210}Pb and MHs

As noted earlier, no physicochemical data are available from the MH soil cores. Therefore, some assumptions are necessary for estimating and comparing OC burial rates between the MH and ^{210}Pb techniques. We assumed that the OC density of the MH cores was the same as that of the ^{210}Pb cores, which is supported by both regional and national observations that OC density in tidal wetlands does not have a depth trend (Breithaupt et al., 2014; Holmquist et al., 2018). Therefore, if the MH accretion rate was 50% of the ^{210}Pb accretion rate for the corresponding time interval, we assumed that the MH OC burial rate was also 50% of the ^{210}Pb OC burial rate.

2.3.4. Calculation of Burial Rates

Soil mass accumulation rates (g m^{-2} year^{-1}) for core intervals were calculated by dividing DBD (g cm^{-3}) by the age at the bottom of the interval (years), with age determined using one of the three chronometers noted

Table 1
Mean (±1 SE) Soil Physicochemical Characteristics Over Soil Depths Corresponding to the Depth of Excess ^{210}Pb for Each Core

	NMg1	NMg2	NMg3	SMg1	SMs1	SMg2	SMs2
DBD (g cm^{-3})	0.29 (0.03) a	0.31 (0.02) a	0.20 (0.01) b	0.11 (0.00) b	0.10 (0.00) b	0.19 (0.01) b	0.13 (0.01) b
SOM (%)	39.8 (3.5) a	33.8 (1.4) a	39.1 (1.2) a	83.7 (0.4) b	82.5 (0.4) b	63.1 (1.3) c	79.2 (0.1) b
NC-Mineral (%)	40.8 (4.2) a	47.7 (1.9) a	34.5 (1.8) a	8.5 (0.5) bc	9.8 (0.8) bc	19.0 (1.9) c	3.9 (0.6) b
Lignin (%)	1.2 (0.1) a	0.8 (0.2) a	1.2 (0.0) a	1.6 (0.7) a	1.4 (0.1) a	0.9 (0.3) a	3.5 (0.4) b
OC (%)	18.1 (1.7) a	15.1 (1.1) a	18.9 (0.5) a	42.3 (0.4) b	43.6 (0.5) b	29.6 (0.3) c	39.0 (0.5) b
TN (%)	1.1 (0.1) ab	0.8 (0.1) a	1.0 (0.0) a	2.1 (0.1) c	2.6 (0.0) c	1.4 (0.0) bc	2.1 (0.0) c
TP (mg g^{-1})	0.53 (0.07) bc	0.81 (0.02) cd	0.57 (0.02) bce	0.59 (0.03) bce	0.79 (0.04) bcd	0.92 (0.03) d	0.34 (0.05) a
OC:TN (mol mol^{-1})	20.9 (0.3) ac	23.1 (0.6) ab	23.4 (0.2) ab	23.2 (1.0) ab	19.3 (0.2) c	24.2 (0.4) b	21.9 (0.4) ab
TN:TP (mol mol^{-1})	52.5 (11.4) a	20.3 (1.3) b	37.1 (1.3) a	81.3 (3.0) ac	73.8 (4.7) a	34.4 (0.8) a	147.2 (17.1) c
δ^{13}C (‰)	−27.3 (0.1) a	−27.4 (0.0) a	−28.0 (0.1) b	−28.0 (0.2) b	−27.2 (0.2) a	−27.4 (0.1) a	−27.3 (0.2) a
δ^{15}N (‰)	1.6 (0.1) a	1.8 (0.0) ab	1.5 (0.0) a	2.0 (0.2) ab	3.1 (0.2) b	2.1 (0.1) ab	1.4 (0.4) a

Note. Different lowercase letters within each row indicate a significant difference among sites ($p < 0.05$); if any letters between sites are the same, then there is no significant difference. DBD = dry bulk density; SOM = soil organic matter; NC-mineral = noncarbonate.

previously. Burial rates (g m^{-2} year^{-1}) of constituents such as OC, lignin, or NC-mineral were calculated by multiplying their respective fractions of total soil mass by an interval's mass accumulation rate.

2.4. Soil Composition

Measurements of OC, TN, total phosphorus (TP), δ^{13}C, δ^{15}N, and lignin were conducted for core intervals for which ^{210}Pb dates were available (up to ~120 years). Nutrient and stable isotopes for the southern region samples were analyzed at Southern Cross University. Nutrient and stable isotope samples from the northern region sites were analyzed at the University of Florida, except for TP analyses, which were conducted at the University of Central Florida. Lignin content was measured using two different methods. Measurements for the southern region cores were conducted at University of Central Florida and consisted only of total lignin; measurements for the northern region cores were conducted at University of Florida and consisted of total lignin and lignin phenols. There is some uncertainty associated with using two different methods; however, results were consistent and similar between methods (Table 1).

2.4.1. Southern Region Soil Composition Analyses

Samples of OC, TN, and their stable isotopes were analyzed with a PDZ Europa Automated Nitrogen Carbon Analyzer-Gas Solids Liquids elemental analyzer connected to a PDZ Europa 20-20 isotope ratio mass spectrometer. Analytical precision was 0.28% for C, 0.02% for N, 0.2‰ for δ^{13}C, and 0.3‰ for δ^{15}N. Samples were acidified by hydrochloric acid (HCl) fumigation in a desiccator to remove inorganic carbon prior to measurements of OC and δ^{13}OC (Harris et al., 2001). TP for the southern region sites was measured using a Perkin Elmer ELAN Dynamic Reaction Cell-equipped Inductively-Coupled Plasma Mass Spectrometer.

For the southern region sites, total lignin content was measured using a filtration modification of the acetyl bromide method (Moreira-Vilar et al., 2014). Subsamples (0.3–0.5 g) of freeze-dried, homogenized soil were weighed into centrifuge tubes. A sequence of solvents was added to the samples, agitated, allowed to soak for 10 min, then centrifuged and decanted into funnels fitted with preweighed G/FA grade glass fiber filters (1.6 μm). The solvents were 20 ml 0.05 M potassium phosphate, 21 ml 1% Triton X-100, 14 ml 1 M NaCl, 14 ml nanopure water, and 10 ml acetone. The sediment that was retained on the filter was oven dried at 70 °C overnight. A 0.02 g subsample was then weighed into centrifuge tubes followed by addition of 0.5 ml 25% acetyl bromide before being incubated at 60 °C for 1 hr. Samples were cooled in a refrigerator for 10 min to slow the incubation, after which 0.9 ml 2 M sodium hydroxide (NaOH), 0.1 ml 5 M hydroxylamine-HCl, and 0.5 ml glacial acetic acid were added. Samples were diluted with nanopure water (20:1) because of the high lignin content and absorbance measured on a BioTek Synergy HTX microplate reader (BioTek Instruments Inc., Winooski, VT) at 280 nm. Soil concentrations were determined using a calibration curve created from certified reference material of 10.4 ± 0.4 mg lignin L^{-1} (Sigma-Aldrich, Lot LRAB1799).

2.4.2. Northern Region Soil Composition Analyses

Measurements of OC, TN, and stable isotopes for the northern region soil samples were obtained using a Carlo Erba 1500 CN elemental analyzer coupled to a Thermo Electron DeltaV Advantage isotope ratio mass spectrometer. Samples were treated using HCl acid fumigation prior to OC and δ^{13}OC analysis to remove any inorganic carbon present (Harris et al., 2001). Analytical precision was 0.31% for C, 0.11% for N, 0.11‰ for δ^{13}C, and 0.07‰ for δ^{15}N. TP for the northern region sites was measured following the protocol of Andersen (1976) by digesting precombusted samples in 1 M HCl and analyzing the digestant colorimetrically with a SEAL AQ2 Automated Discrete Analyzer (Seal Analytical, Mequon, WI) using EPA method 365.1 Rev. 2.0 (USEPA 1993).

Lignin-phenols from the northern samples were extracted and analyzed, along with other cupric oxide (CuO) oxidation products, from freeze-dried soil using the cupric oxide method of Hedges and Ertel (1982), modified by Louchouarn et al. (2010) and reported in detail in Shields et al. (2019). Briefly, enough soil for 3–5 mg of OC was oxidized in a modified gas chromatograph oven for 3 hr at 150 °C using reaction vessels that contained soil, a stainless-steel ball bearing, cupric oxide (CuO) powder, ferrous ammonium sulfate hexahydrate, and N_2-sparged 2 N NaOH. Following oxidation, an internal recovery standard mix (0.5 μg/μl ethyl vanillin and 0.5 μg/μL 4-methoxycinnamic acid) was added to each vessel. Vessels were vortexed to loosen the ball bearing before centrifuging again. Supernatant was decanted into Pyrex screw-top test tubes with PTFE-lined caps. Vessels were rinsed twice with 1 N NaOH and centrifuged and decanted following each rinse into the respective screw-top test tubes. Extracts in each tube were acidified to a pH less than 2 using 6 N HCl, supersaturated with NaCl, and left to rest overnight at 4 °C. The salting-out extraction was finished the following day with the addition of ethyl acetate and the centrifugation. The ethyl acetate layer on top was pipetted through a sodium sulfate column into scintillation vials, which were later dried down under a gentle stream of N_2 to ~1 ml volume, transferred to a 4 ml vial using three additional ethyl acetate rinses of the 20 ml scintillation vial, and blown down to completion under N_2. Dried lignin extracts were dissolved in pyridine and were derivatized with the addition of N,O-bis (trimethylsilyl) trifluoroacetamide. The derivatized extract was analyzed on a Thermo Scientific Trace 1310 Gas Chromatograph coupled to a Thermo Scientific TSQ8000 Triple Quadrupole Mass Spectrometer with an Agilent DB-5 ms column (30 m length and 0.25 mm internal diameter).

The eight major lignin oxidation products are vanillin, acetovanillone, vanillic acid, syringealdehyde, acetosyringone, syringic acid, p-hydroxycoumaric acid, and ferulic acid. Additional CuO oxidation products include 3,5-dihydroxybenzoic acid, p-hydroxybenzaldehyde, p-hydroxybenzoic acid, and p-hydroxyacetophenol (PON). These compounds were detected and quantified using selected reaction monitoring. Relative response factors were normalized to an analytical standard (Methyl 3,4-dimethoxybenzoate) to account for instrument variability. Phenol concentrations were additionally corrected for loss during the extracting using the ethyl vanillin and 4-methoxycinnamic acid recovery standards; samples with lower than 50 % recovery were reextracted.

2.5. Data Analyses
2.5.1. IFs

As noted in section 1.1, much of the data about sediment accumulation in coastal wetlands is based on long-term average rates. Our dating approach (section 2.3) allows us to evaluate fine-scale temporal changes in these rates. Annual rates of apparent acceleration (g m^{-2} year^{-2}) were calculated as the slope of the burial rate as a function of time since the oldest depth in the core (i.e., change in burial rate as a function of time). Second, to quantify the magnitude of change that occurred over ~100–120 years, increase factors (IFs) were calculated by dividing the average (μ) rate of the top two intervals (μ_T) by the average rate of the bottom two intervals (μ_B) for each core.

$$IF_{Pb-210} = \frac{\mu_T}{\mu_B} \tag{1}$$

Two points from the top and bottom of the cores were used to avoid a single point providing an unusually high or low estimate of the burial rate at each depth. As described in section 2.3, short-term rates derived from ^{210}Pb may differ from those derived from the MH technique over corresponding time periods. Therefore, an $IF_{MH/Pb-210}$ was calculated in addition to the IF_{Pb-210}

$$IF_{MH/Pb-210} = \frac{\mu_{MH}}{\mu_B} \tag{2}$$

where the numerator (μ_{MH}) is the MH-derived rate and μ_B is the same as in equation (1). These surface and bottom average rates for equations (1) and (2) are provided in Table S1. A value greater than 1 equates to an increase, and a value less than 1 equates to a net decrease in the past century.

The $IF_{MH/Pb-210}$ considers whether a second tool for measuring recent, surficial rates concurs with the rate of increase observed solely with ^{210}Pb. A similar exercise could be conducted with ^{137}Cs (for the three cores where a peak in activity was discernible). The close agreement between the 50 year depths of the two methods indicates those IFs would be the same and therefore are not discussed further here. It should be noted that the lack of another, independent chronometer at the 100–120 year timescale means that we are unable to provide an alternative perspective on soil ages at the bottom of these cores.

2.5.2. Vertical Profiles of Lignin:OC

In order to test the hypothesis that postdepositional degradation contributes to the appearance of acceleration in OC burial rates, we interpreted a vertical lignin: OC profile to indicate that the proportions of stable and unstable components have remained constant between younger and older soils, suggesting no preferential or additional degradation with depth. This prediction is based on the expectation that lignin is relatively stable over the timescales of observation used here. Conversely, a negative slope in the lignin: OC profile indicates that lignin represents a larger proportion of the OC pool in older samples than in younger samples, suggesting that postdepositional degradation has preferentially decreased the overall OC pool in the oldest, deepest samples. A counterinterpretation that a change in dominant organic matter source could be responsible for the negative lignin: OC slope is not expected at these sites as they represent historically stable mangrove and marsh locations. However, a temporal change from herbaceous to woody or algal inputs should be readily identified by the OC:TN, $\delta^{13}C$, and $\delta^{15}N$ values (e.g., Sanders et al., 2014) and the lignin phenol ratios (e.g., Hedges et al., 1988).

2.5.3. Lignin Phenol Ratios

To complement assessment of the degradation state of the soil based only on lignin: OC, the acid-to-aldehyde ratios of vanillyls and syringyls ((Ad:Al)$_v$ and (Ad:Al)$_s$, respectively) and the ratio of p-hydroxyl phenols (p-hydroxybenzaldehyde, p-hydroxybenzoic acid, and PON) to the sum of vanillyls and syringyls (P:(S + V)) are used as indicators of lignin oxidation by fungi and other microbes (Opsahl & Benner, 1995; Otto & Simpson, 2006). Ratios of S:V can be used in combination with (Ad:Al)$_s$ to look at preferential S phenol degradation. The combination of these two parameters helps differentiate whether S:V changes are related to source or degradation. For (Ad:Al)$_v$, fresh tissues are typically <0.3, and highly degraded materials (via oxidative degradation) have ratios >0.6 (Hedges et al., 1998). In addition, the fractionation of lignin phenols from their solubilization from plant litter and subsequent sorption to soils has been shown to increase (Ad:Al)$_v$ to values much greater than 0.6 (Hernes et al., 2007). For (Ad:Al)$_s$, leaching and sorption effects also produce values in excess of 0.6 (Hernes et al., 2007), with fresh tissues and highly degraded tissues having ratios <0.14 and > 0.16, respectively (Hedges et al., 1998). Similar to Ad:Al, P: (S + V) is often used as a proxy for degradation in soils but for the demethylation of V and S phenols due to brown rot fungi (Jex et al., 2014). The P phenols have been found in the oxidation products of protein-rich organisms such as plankton and bacteria, so this proxy may not fully reflect lignin degradation (Jex et al., 2014). To determine whether the P phenols are reflective of lignin-derived decomposition, we employed the ratio of p-hydroxyacetophenone (PON) to TP phenols. PON is derived predominantly from lignin, whereas p-hydroxybenaldehyde and p-hydroxybenzoic acid, the other two P phenols that compose TP, are released by nonlignin sources (Benner et al., 1990). Thus, a high ratio of PON:P would indicate that P: (S + V) can be used as a proxy for degradation via brown rot fungi demethylation, whereas a low PON:P would indicate that P: (S + V) is more reflective of nonlignin derived material.

2.5.4. Statistical Analyses

Statistical analyses were carried out using IBM SPSS Statistics Version 25. Differences for average soil characteristics by site were conducted with Welch's one-way ANOVA and post hoc Games-Howell comparisons ($\alpha = 0.05$); these procedures were used because the homogeneity of variance assumption was not met for all sites with data transformations. Data were treated with a log normal or fourth root transformation to meet the normal distribution assumption. Three of the soil variables (TN, TN:TP, and $\delta^{15}N$) could not be transformed to meet the normality assumption, and comparisons were made using the nonparametric
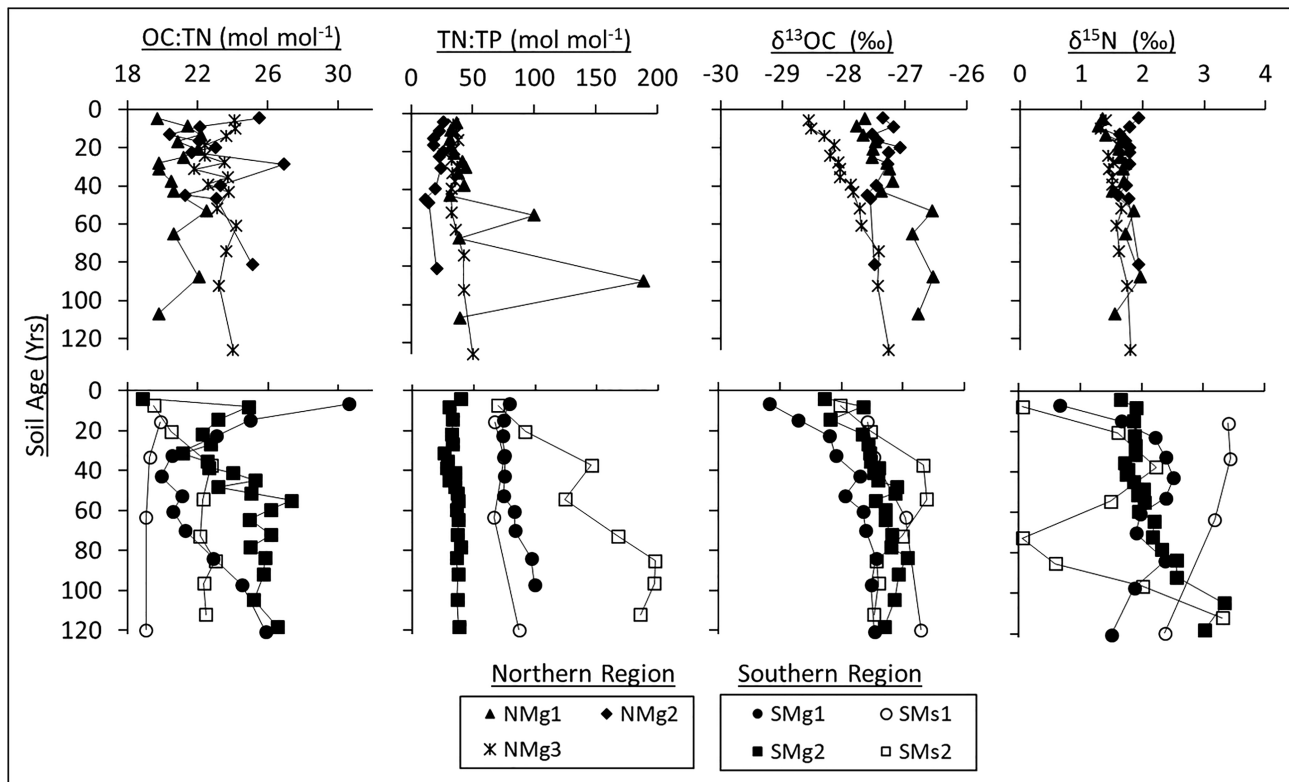
Figure 2. Core profiles of organic carbon to total nitrogen (OC:TN) ratios, total nitrogen to total phosphorus (TN:TP) ratios, δ^{13}OC, and δ^{15}N as a function of soil interval ages (derived from ^{210}Pb).

Kruskal-Wallis H test and post hoc median comparisons ($\alpha = 0.05$). Uncertainty terms throughout this communication represent 1 standard error of the mean, unless stated otherwise.

3. Results

3.1. General Soil Characteristics

Comparison of soil characteristics between sites indicated that the temporal phenomenon of increasing OC burial rates in the past century is not isolated to one particular region or soil type. Soil DBD was similar across sites, ranging from 0.10 ± 0.00 g cm^{-3} at SMs1 to 0.31 ± 0.02 g cm^{-3} at NMg2 (Table 1). The SOM content was not different between all sites but varied from a low of 33.8–39.8 % at the three northern sites, to 63.1 % at SMg2, to a range of 79.2–83.7% at SMs2 and SMg1, respectively ($p < 0.05$). Similarly, NC-mineral content varied considerably, ranging from a low of 3.9 ± 0.6% at SMs2 to a high of 47.7 ± 1.9% at NMg2. Total lignin content was greatest at site SMs2 (3.5 ± 0.3%) ($p = 0.000$) and ranged from 0.8 ± 0.2% to 1.6 ± 0.7% at the remaining sites. Despite the differences in SOM content, site mean OC:TN showed relatively little variability (range 19.3 ± 0.2 at SMs1 to 24.2 ± 0.4 at SMg2). There was no consistent positive or negative trend in OC:TN by soil age for these sites (Figure 2). The most stable over the past 120 years was marsh core SMs1, with OC:TN values near 19 throughout. The other marsh core, SMs2, was largely stable around 22 historically followed by a decrease to near 18 in the most recent decade; a similar pattern was seen in core SMg2, with historical stability around 26, followed by a decrease to near 18 in the surface interval. The OC:TN of SMg1 fluctuated the most (the coefficient of variation was 0.14 compared to an average of 0.05 for the other cores), with values near 26 at the 120 year depth that decreased steadily to near 20 at the 40 year soil age, and then subsequently increased to over 30 in the surface interval. The three cores from the northern region lacked clear directional trends in OC:TN but had extensive fluctuations between intervals.

TP ranged from 0.34 ± 0.05 mg g^{-1} at SMs2 to 0.92 ± 0.03 mg g^{-1} at SMg2. There was substantial variation in TN:TP, from a low of 20.3 ± 1.3 mg g^{-1} at NMg2 to a high of 147.2 ± 17.1 mg g^{-1} at SMs2. The TN:TP profiles
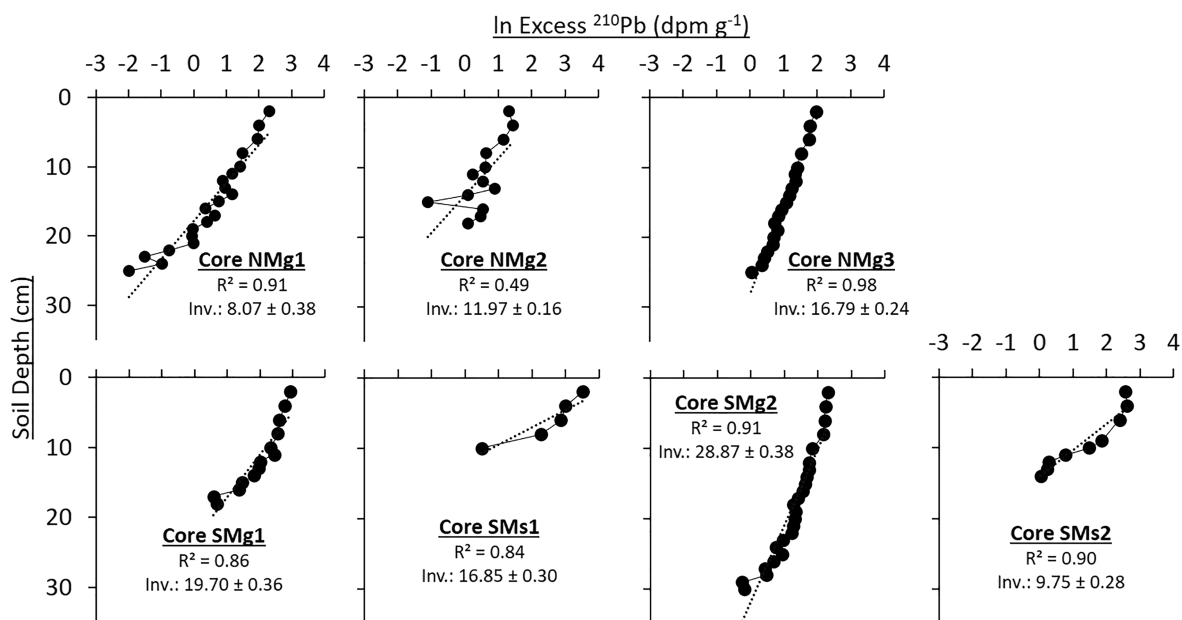
Figure 3. Core profiles of ln Excess ^{210}Pb Activity versus soil depth; Inv. stands for Inventory (dpm cm^{-2}).

for cores SMg2, SMg1, and SMs1 were relatively unchanging over the past century. The lowest values, equating to the least P-limitation, occurred in core SMg2, the site nearest to the Gulf of Mexico. Cores SMg1 and SMs1, which are relatively close to one another, had similar TN:TP over the past century. Site SMs2 showed very high P-limitation 120–80 years ago, followed by a steady decrease to near 70 in the most recent decade. The three northern region sites showed similar vertical trends with relatively low TN:TP, except for some very high variation in two of the intervals in core NMg1 (Figure 2).

Mean δ^{13}C values were similar across sites, with a range of −28.0‰ to −27.2‰ (Table 1). The δ^{13}C profiles of all sites indicate a down-core enrichment of 1.0–1.5‰ over the past 100–120 years (Figure 2). Mean δ^{15}N values ranged from 1.4‰ at SMs2 to 3.1‰ at SMs1 (Table 1). The δ^{15}N profiles of the northern region sites are extremely consistent, ranging only between 1.0‰ and 2.0‰ over the past 100–120 years. In contrast, the values for the southern region sites exhibited high temporal variability (Figure 2).

3.2. Age-Depth Profiles: ^{210}Pb, ^{137}Cs, and MHs

Excess ^{210}Pb activities reached depths ranging from 10 cm (SMs1) to 31 cm (SMg2) (Figure 3). The cores exhibit various degrees of a linear decrease with depth, indicative of variable sedimentation rates over time. A mixed surface layer may be present in the top four intervals of SMg2 and top two intervals of SMs2 that may be caused by physical mixing or bioturbation from crab burrowing. Core NMg2 showed the weakest correlation coefficient ($R^2 = 0.49$), indicative of the highly variable sedimentation rates over the core's history. Core inventories of excess ^{210}Pb (dpm cm^{-2}) generally fit three groups (Figure 3), indicating that the phenomenon of increasing burial rates has occurred at sites with variable inventories across the region. The first grouping was the lowest and ranged from 8.07 ± 0.38 to 11.97 ± 0.16 dpm cm^{-2} for cores SMs2, NMg1, and NMg2. The second inventory grouping included sites SMg1, SMs1, and NMg3 and ranged from 16.79 ± 0.24 to 19.70 ± 0.36 dpm cm^{-2}. The highest inventory was 28.87 ± 0.38 dpm cm^{-2} at SMg2. We interpret the low values as the regional average based on atmospheric deposition, with higher inventories at the other sites indicative of more regular allochthonous sediment deposition. Of the four southern region cores, the depth interval closest to 120 years old was 17 cm in SMg2 (118 years), 13 cm in SMs2 (112 years), 16 cm in SMg1 (120 years), and 8 cm in SMs1 (120 years); in the northern cores, the depths were 23 cm in NMg1 (107 years), 18 cm in NMg2 (104 years), and 24 cm in NMg3 (126 years). All interval dates and associated age errors are provided in the archived data set (https://doi.org/10.25573/data.9894266).

Of the seven cores, only SMs1, SMs2, and NMg3 had discernible ^{137}Cs peaks, though the profile for NMg3 indicates a substantial amount of upward mobilization from the peak (Figure 4). The SMs1 peak occurred
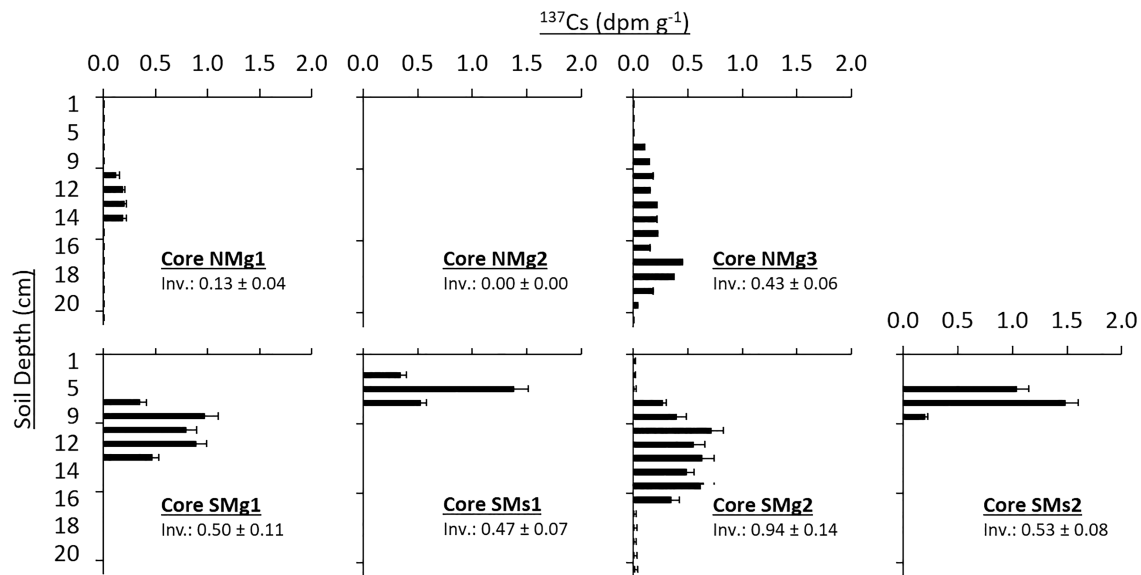
Figure 4. Core profiles of ^{137}Cs activities versus soil depth. Only SMs1, SMs2, and NMg3 exhibited discernible activity peaks. Inv. stands for Inventory (dpm cm^{-2}).

in the 4–6 cm interval (1.36 ± 0.06 dpm g^{-1}), the SMs2 peak occurred in the 6–8 cm interval (1.48 ± 0.06 dpm g^{-1}), and the NMg3 peak occurred in the 16–17 cm interval (0.44 ± 0.03 dpm g^{-1}). Cores SMg1, SMg2, and NMg1 had ^{137}Cs activities but no discernible peaks. Of the cores with ^{137}Cs activity, total inventories ranged from 0.13 ± 0.04 dpm cm^{-2} in NMg1 to 0.94 ± 0.14 dpm cm^{-2} in SMg2. There was no inventory of ^{137}Cs discernible in core NMg2.

Trends from the MH stations exhibited varying periods of accretion, stationarity, or erosion over the different record lengths (Figure 5). Long-term trends were relatively similar among sites, ranging from 2.47 ± 0.34 and 2.47 ± 1.17 mm year^{-1} at SMg/Ms1 and NMg3, respectively (Figures 5c and 5d) to 4.18 ± 2.40 mm year^{-1} at SMg2 (Figure 5e). However, site SMg 2 shows a strong positive influence from Hurricane Irma's storm surge deposition, and the rate was 0.86 ± 0.32 mm year^{-1} when those storm-influenced sampling points were removed. There was considerable variability between MH plots within sites. The largest difference occurred at SMs2, where the lowest plot trend was 2.32 mm year^{-1} and the maximum plot trend was 4.42 mm year^{-1}, a difference of 2.10 mm year^{-1} (Figure 5f). The average of the difference between the maximum and minimum plot trends for the six sites was 1.40 ± 0.25 mm year^{-1}. When data from 2017 and 2018 were withheld from the southern region sites (for comparison with equivalent time periods of ^{210}Pb rates), the adjusted rates were are as follows (linear trend, minimum plot trend, and maximum plot trend): (a) SMg/Ms1: 2.23 ± 0.19, 2.01, and 2.36 mm year^{-1}; (b) SMg2: 0.86 ± 0.32, 0.21, and 1.88 mm year^{-1}; and (c) SMs2: 0.88 ± 0.32, 0.72, and 1.48 mm year^{-1}.

The three cores with discernible ^{137}Cs peaks showed good agreement with the depth of the 1963 peak identified by the ^{210}Pb CRS model (Figure 6a), with each occurring along the 1:1 line. There was less agreement between the short timescale ^{210}Pb rates and MH accretion rates (Figures 6b and 6c). When using the complete MH record, the MH accretion rate exceeded the ^{210}Pb rate by 1.2 and 0.6 mm year^{-1} at sites SMs1 and SMs2, respectively, while site SMg1 essentially matched the MH accretion rate with a slight difference of 0.2 mm year^{-1} (Figure 6b). The four remaining sites had ^{210}Pb rates that exceeded MH accretion rates; on average, ^{210}Pb accretion rates were 0.7 ± 0.5 mm year^{-1} greater than those for the MH method when using the complete MH record. The difference was even greater (1.6 ± 0.6 mm year^{-1}) when comparing accretion rates for only equivalent time periods (Figure 6c). The difference at individual sites ranged from -0.9 ± 0.2 mm year^{-1} (i.e., the MH accretion rate was greater than the ^{210}Pb rate) at site SMs1 to 4.0 ± 0.8 mm year^{-1} at site SMg2.

3.3. Burial Rate Profiles: OC, Lignin, Lignin:OC, and NC-Mineral

All seven cores exhibited significant, positive trends of apparent acceleration in OC burial over the past 100–120 years ($p < 0.05$; Figure 7). The strongest acceleration occurred in core SMg2, with an increase of $1.63 \pm$
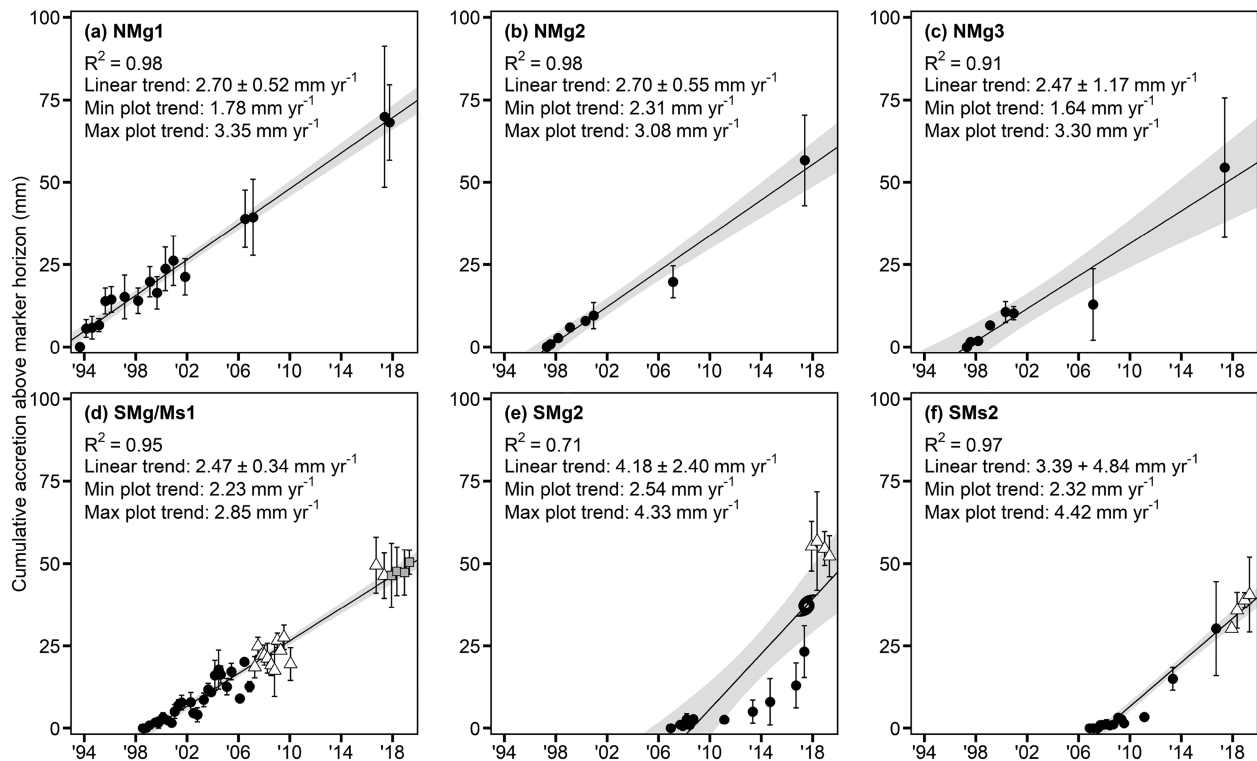
Figure 5. Time series of cumulative accretion above feldspar surface marker horizons (MHs) for each site (panels a - f). Reported values in the upper left of each panel represent the linear trend (i.e., the plotted trend line), as well as the minimum and maximum long-term trends derived from individual MHs at each site. Southern region sites are composed of multiple horizon placements over this time period (indicated by different symbols); northern region sites are based on a single MH placement. Hurricane symbol in (b) indicates influence of Hurricane Irma (September 2017) on elevated accretion at site SMg2.

0.11 g OC m^{-2} year^{-2} ($p < 0.001$). The slowest increase occurred in core SMs2, with 0.25 ± 0.08 g OC m^{-2} year^{-2} ($p = 0.018$). The weakest correlation coefficient ($R^2 = 0.45$) and highest slope uncertainty (0.99 ± 0.31 g OC m^{-2} year^{-2}) occurred at NMg2. The 100 year average OC burial rates ranged from a low of 29.7 g m^{-2} year^{-1} in core SMs1 to a high of 136.5 g m^{-2} year^{-1} in core SMg2 (Table S2). The lowest 100 year average OC burial rates occurred in the two marsh cores, with rates of 29.7 and 49.3 g m^{-2} year^{-1} for SMs1 and SMs2, respectively. The highest OC burial rates occurred at site SMg2, with surface burial rates
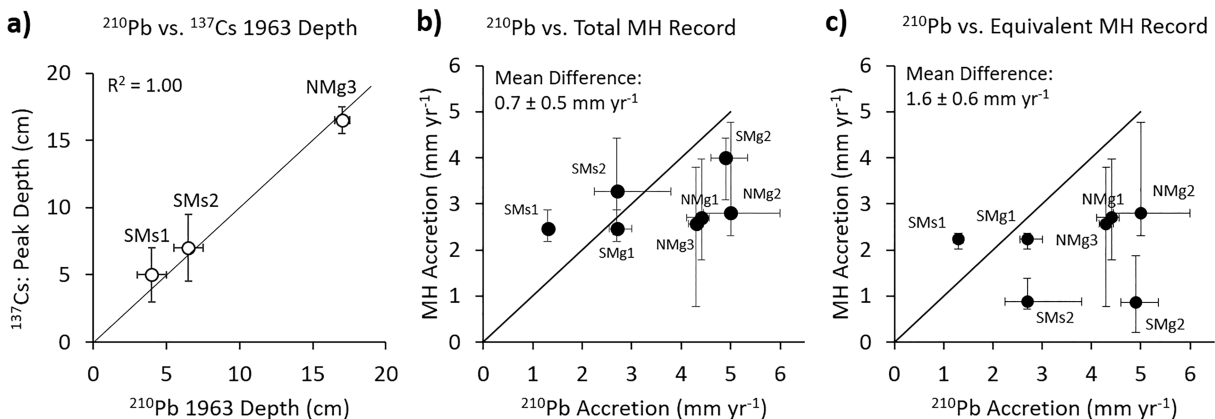

Figure 6. Comparison of ^{210}Pb, ^{137}Cs, and marker horizons (MHs). (a) The depth to 1963 using the ^{210}Pb CRS dating model and ^{137}Cs for the three cores with discernible ^{137}Cs peaks, (b) accretion rate comparison between the complete MH record and ^{210}Pb accretion rates with start dates corresponding to the beginning of each MH record, and (c) accretion rate comparison between the MH and ^{210}Pb over time periods with roughly equivalent start and end dates (see section 2). Black lines in each panel represent 1:1 line.
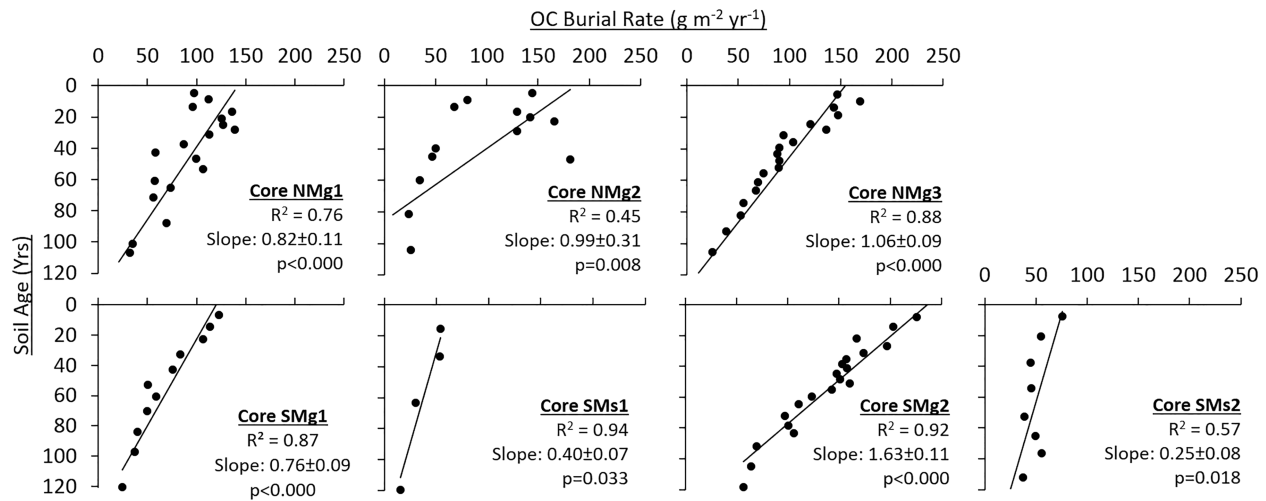
Figure 7. Core profiles of organic carbon (OC) burial as a function of ^{210}Pb-derived soil age. The slope represents the annual rate of OC burial change over the dated record.

near 250 g m^{-2} year^{-1}. The IF$_{Pb-210}$ in OC burial rates (see section 2.5) was lowest in the two marsh cores (1.4 and 2.4 for SMs2 and SMs1, respectively) and was highest in core NMg3 (6.2; Table 2). If the mean MH rates are used instead of the surficial ^{210}Pb rates, the IF$_{MH/Pb-210}$ for the SMs2 marsh core decreases to 0.5, the SMs1 core increases to 4.1, and NMg3 decreases to 3.7. The IF$_{MH/Pb-210}$ for cores SMg2 and SMs2 decrease to below 1.0, suggesting no increase in OC burial rates at these sites in the past century.

Four of the seven sites (SMg1, SMg2, SMs2, and NMg3) had significant, positive trends in lignin burial rates (Figure 8). The lowest average lignin burial rates occurred in the marsh cores, with long-term averages of 1.0 and 1.9 g m^{-2} year^{-1}, and the highest long-term average burial rates were in core NMg3 (5.2 g m^{-2} year^{-1}). The IF$_{Pb-210}$ ranged from a low of 1.5 in core NMg1 to a high of 13.1 in core SMg1; it should be noted that the high value for SMg1 was obtained even after excluding the uppermost, high value from core SMg1 (Figure 8). The IF$_{MH/Pb-210}$ for SMg2 and SMs2 both decrease below 1.0 (0.9 and 0.8, respectively), while the IF$_{MH/Pb-210}$ for SMg1 remained high at 12.5 (Table 2). None of the cores showed a significant negative slope in lignin: OC that would indicate preferential degradation at depth compared to the surface (Figure 9). Cores SMg1 and SMs2 had indiscernible trends ($p = 0.034$ and 0.007, respectively (Figure 7).

Deposition rates of NC-mineral sediment varied substantially between cores, from averages of 4.5 and 8.8 g m^{-2} year^{-1} in marsh cores SMs2 and SMs1, respectively, to 187 and 193 g m^{-2} year^{-1} in cores NMg2 and NMg1 (Figure 10). Three of the sites had significant positive, annual increases. The greatest acceleration was 1.17 ± 0.18 g m^{-2} year^{-1} ($p < 0.001$) at NMg3, and the weakest was 0.20 ± 0.03 g m^{-2} year^{-1} at

Table 2
Increase Factors (IFs) (± 1 SE) for Burial Rates of OC, Lignin, Lignin:OC, and NC-Mineral Sediments

Core	IF$_{Pb-210}$				IF$_{MH/Pb-210}$		
	OC	Lignin	Lignin:OC	NC-mineral	OC	Lignin	NC-mineral
NMg1	3.6 (0.5)	1.5 (0.3)	0.8 (0.1)	0.2 (0.0)	2.2 (0.1)	1.3 (0.1)	0.1 (0.0)
NMg2	4.6 (2.4)	4.0 (1.9)	0.8 (0.4)	3.3 (1.6)	2.6 (0.3)	2.2 (0.2)	1.8 (0.2)
NMg3	6.2 (0.7)	5.4 (0.6)	1.0 (0.1)	2.4 (0.3)	3.7 (0.1)	3.2 (0.1)	1.4 (0.1)
SMg1	3.8 (0.6)	13.1 (1.7)	6.7 (0.9)	5.5 (1.0)	3.2 (0.2)	12.5 (0.7)	4.5 (0.3)
SMs1	2.4 (0.2)	2.7 (0.2)	1.1 (0.1)	2.3. (0.2)	4.1 (0.2)	5.4 (0.2)	4.3 (0.2)
SMg2	4.0 (0.6)	5.2 (0.7)	1.2 (0.1)	1.7 (0.2)	0.7 (0.0)	0.9 (0.0)	0.3 (0.0)
SMs2	1.4 (0.5)	2.7 (0.9)	1.9 (0.6)	0.4 (0.1)	0.5 (0.1)	0.8 (0.1)	n/a

Note. See section 2.5.1. Values used in these calculations are provided in Table S1. Lignin:OC is unchanged by the MH-correction.
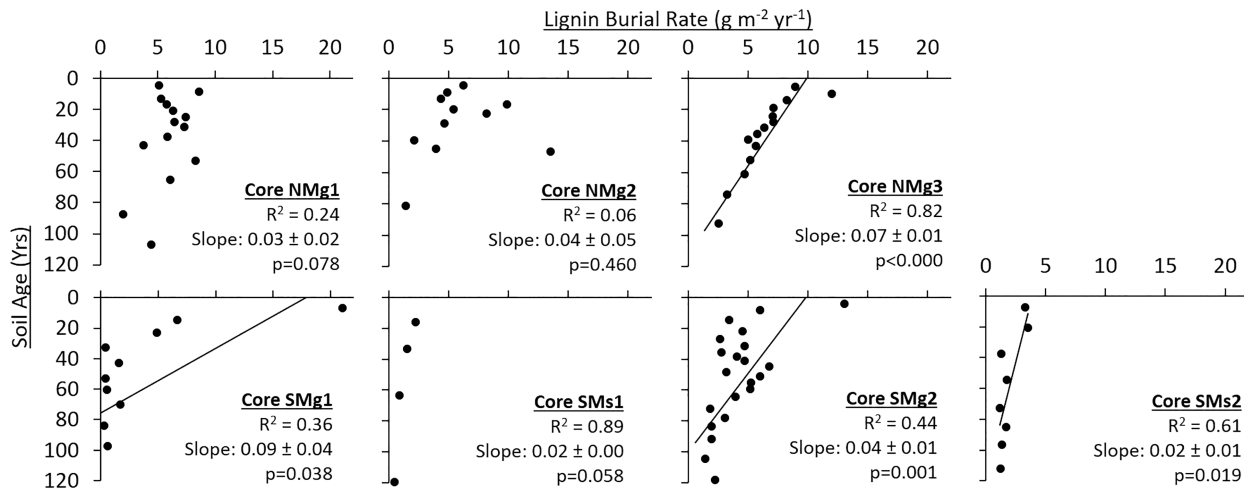
Figure 8. Core profiles of total lignin burial rates as a function of ^{210}Pb-derived soil age.

SMg1 ($p < 0.001$). Site NMg1 showed a significant, negative trend in NC-mineral deposition (-1.70 ± 0.39 g m^{-2} year^{-1}; $p < 0.001$). The IFs for sites SMs2 and NMg2 were 0.4 and 0.2, indicating a decrease in rates over the past century. The decrease in core NMg1 was particularly notable, equating to annual NC-mineral deposition rates in the present day that were ~300 g m^{-2} year^{-1} less than they were a century ago. Aside from the two sites that show IFs less than 1.0 (SMs2 and NMg1), the other sites ranged from 1.7 to 5.5 (Table 2).

3.4. Lignin Oxidation Products

Both (Ad:Al)$_v$ and (Ad:Al)$_s$ for the northern region cores showed some variation with depth that could indicate slight changes in lignin phenol degradation; however, most data points hovered around the median, suggesting relatively uniform V and S phenol degradation over time (Figure 11a). Medians ranging between 0.19 (NMg1) and 0.42 (NMg2) for (Ad:Al)$_v$ fall below what would be expected for highly degraded V phenols (values > 0.6; Hedges et al., 1998) whereas (Ad:Al)$_s$ medians were higher than that expected for highly degraded S phenols (>0.16; Hedges et al., 1998), ranging between 0.20 (NMg1) and 0.31 (NMg3). Decreases in S:V near the surface and relatively stable values throughout the rest of the core profiles (Figure 11c) indicate there was either significant degradation of S phenols compared to V phenols or an increase in angiosperm lignin contributions (S/V > 0.9; Jex et al., 2014) starting around 20 years ago. The P/(V + S) degradation proxy for all three cores increased initially to approximately the 20 year depth and
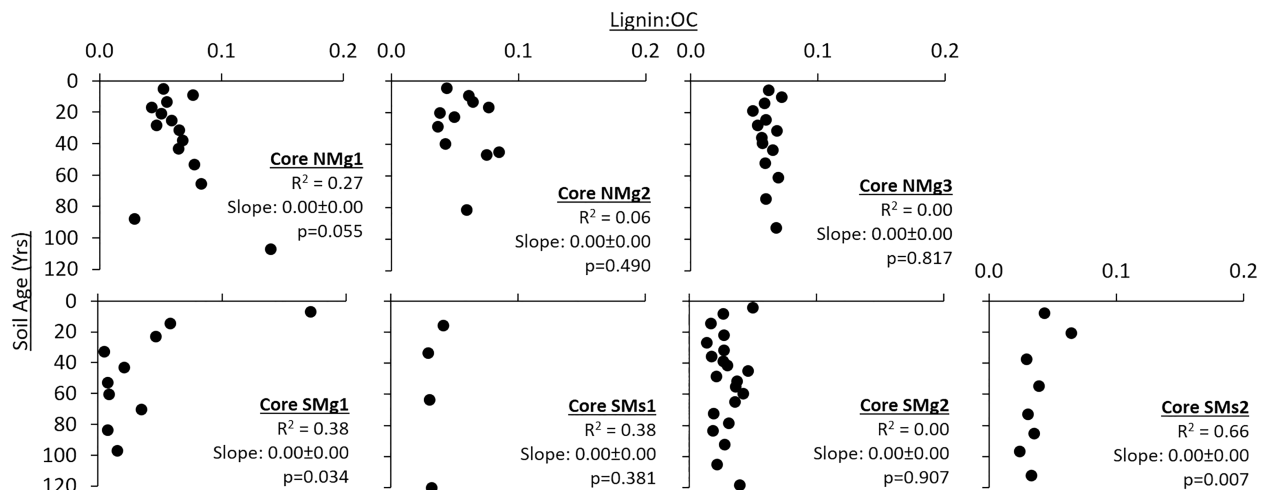

Figure 9. Core profiles of lignin to organic carbon (OC) as a function of ^{210}Pb-derived soil age.
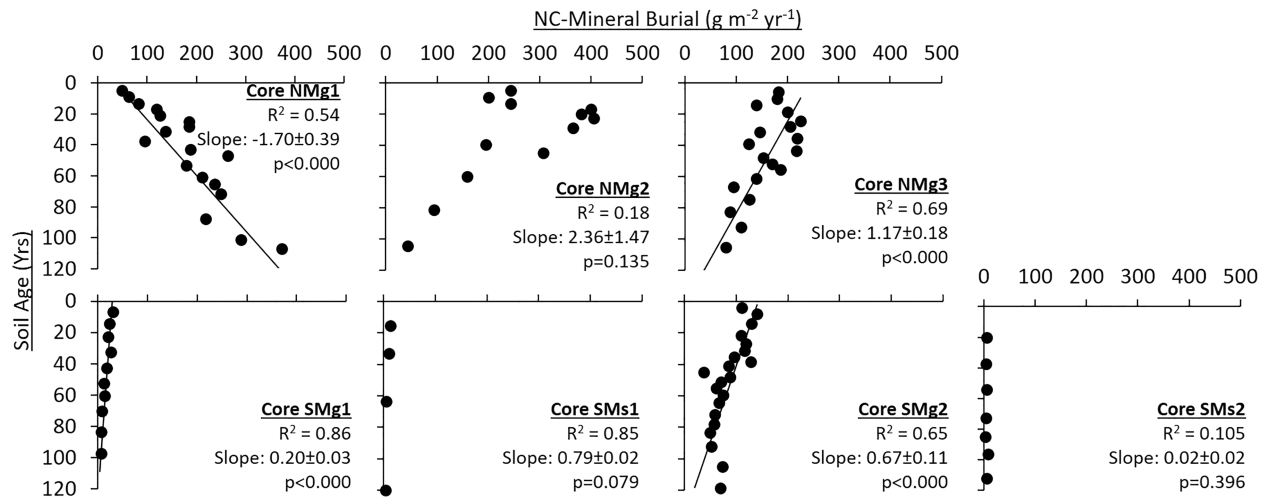
Figure 10. Core profiles of noncarbonate mineral (NC Mineral) burial rates as a function of ^{210}Pb-derived soil age.

then decreased to the surface for each core (Figure 11d). The ratio of PON:P (Figure 11e) was low for all three northern cores (values ranged from 0.09 to 0.19), indicating that either the P phenols are mostly composed of the oxidation products of protein-rich organisms, such as plankton and bacteria (Jex et al., 2014), or there is a lack of demethylation of V and S phenols due to brown rot fungi.

4. Discussion

4.1. Explaining the Apparent Increase in OC Burial Rates

All seven cores exhibited varying increases in OC burial rates by factors ranging from 1.4 to 6.2 over the past 120 years (Table 2 and Figure 7). Based on the combination of evidence discussed below from different
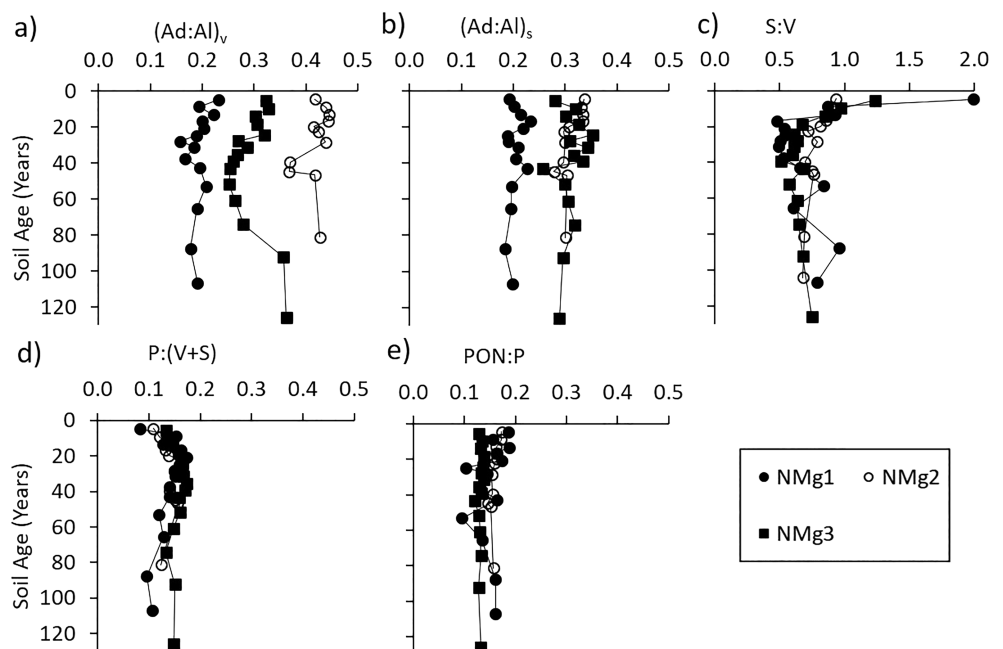
Figure 11. Core profiles of indices of lignin decay as a function of ^{210}Pb-derived soil age for the three northern region cores: (a) acid-to-aldehyde ratios of vanillyls [$(Ad:Al)_v$], (b) acid-to-aldehyde ratios of syringyls [$(Ad:Al)_s$], (c) the ratio of syringyls to vanillyls (S:V), (d) the ratio of p-hydroxyl phenols to the sum of vanillyls and syringyls [P:(S + V)] (note scale difference), and (e) the ratio of p-hydroxyacetophenone (PON) to total P phenols (PON:P).

methods used to measure OC burial, lignin: OC profiles, and indices of lignin decay, we propose that increasing OC burial rates during the past century represent a net acceleration rather than a record influenced by postdepositional degradation of OC or an artifact of the method employed.

4.1.1. Methods for Measuring Burial Rates

A comparison of the overlapping dating methods suggests there is not an anomaly inherent in the ^{210}Pb chronometer, although it potentially overestimates rates compared to the MH approach. For the three cores with identifiable ^{137}Cs peaks (SMs1, SMs2, and NMg3), there was strong agreement with the 1963 soil interval depth as determined by the ^{210}Pb CRS model (Figure 6a), indicating reliability over the 50 year timescale in these cores. The depth of the 1963 interval occurred at 4–6, 6–9, and 17–18 cm in the three cores, demonstrating that the two radionuclides agreed over a relatively broad range of accretion rates. These three cores have the lowest salinity conditions, with the two marsh sites being mostly freshwater and occasionally brackish (Jiang et al., 2013; Saha et al., 2012) and the mangrove core being heavily influenced by managed freshwater discharges from Picayune Strand State Forest. The observation that clear ^{137}Cs peaks are only visible in the cores from more freshwater conditions supports findings of the limited utility of ^{137}Cs in saline peat soils (Corbett & Walsh, 2015; Drexler et al., 2018; Lynch et al., 1989; Marchio et al., 2016).

Comparisons across sites indicate that ^{210}Pb rates are greater than MH rates by 1.6 ± 0.6 mm year^{-1} over 5–25 year soil depths (Figure 6c). However, both MH and ^{210}Pb techniques can have substantial spatial uncertainties. The difference in accretion rates of individual MH plots across these sites averaged 1.40 ± 0.25 mm year^{-1}. Previous ^{210}Pb measurements in ENP found a difference of 2.3 mm year^{-1} between minimum and maximum 10 year accretion rates for six cores within a 200 × 200 m footprint in ENP (Breithaupt et al., 2014). These comparisons demonstrate the substantial and omnipresent spatial variability in accretion and OC burial rates in these wetlands. The MH-^{210}Pb IFs for each site (Table 2) represent a conservative estimate; we suggest they should not be viewed as an alternative to ^{210}Pb IFs, but rather, the two should be viewed together as a range of potential increases. Some discrepancy between rates derived from these two methods could be that ^{210}Pb rates typically extend deeper into the soil profile than MH cores and therefore may include a greater contribution from root growth. However, this is unlikely to be the case here, because our comparisons are for comparable soil depths. There is also likely to be some difference between methods because the dates used to estimate accretion for the ^{210}Pb intervals are not identical to those of the MH intervals. At these sites, discrepancy between the methods can most likely be attributed to the distance between sampling points. Although measurements from both methods were collected at the same site, there are noticeable microtopographic differences visible across this landscape. The best way to ensure comparison of equivalent material would be to collect a ^{210}Pb core from within the MH plot so that the depth intervals above and below the feldspar layer could be dated and compared directly with the date of MH deposition.

4.1.2. Indicators of Postdepositional Mineralization

The lignin phenol data support the occurrence of uniform OC degradation over the past century, as indicated by relatively consistent (Ad/Al)$_v$ values. These (Ad/Al)$_v$ values are typical of low to moderately degraded soils (values < 0.3–0.6; Hedges et al., 1998). Decreases in S/V values near the surface (Figure 11c), however, suggest there has been preferential biotic decay of S phenols over V phenols (Hedges et al., 1998; Opsahl & Benner, 1995) with potentially high S phenol degradation starting near the surface. S/V values can be as high as 5.2 (Jex et al., 2014); thus, the maximum value of 2.0 at the surface of NMg1 could still suggest there has been greater degradation of S phenols over V phenols during initial OC deposition. Uniform (Ad/Al)$_s$ values greater than 0.16 in all three cores suggest high S phenol degradation (Hedges et al., 1998), with little or no change in the preference for S phenol degradation over V phenol degradation over time. The higher (Ad/Al)$_v$ and (Ad/Al)$_s$ values for NMg2 and NMg3 could be related to leaching of the phenols from plant litter and their sorption to the soils (Hernes et al., 2007) given that these sites appear to receive more tidal flushing (based on anecdotal field observations) than the mangrove basin site (NMg1) that is rarely inundated at high tide.

Although sites NMg1 and NMg2 had lignin: OC IFs less than 1.0 (Table 2), the trends for the complete core profiles were not significantly different from zero (p = 0.06 and 0.49, respectively; Figure 9). This lack of significant changes in lignin: OC combined with the lignin phenol data is interpreted as a lack of evidence for postdepositional OC mineralization as the driver of increased OC burial rates at these sites (Figure 7).

Similarly, the profiles of the remaining cores did not show evidence of changing lignin: OC with age/depth. According to our research hypothesis, the stable lignin: OC profiles indicate consistent and uniform postdepositional mineralization of soil OC and total lignin over the past century.

The soil nutrient ratios and stable isotopic composition did not suggest that a diagenetic effect is responsible for the increase in OC burial rates. For the three northern region cores and SMg1, ratios of OC:TN were variable over the dated record, with no positive or negative trends. There was a decrease of less than 1.0 in OC: TN for SMs1, while SMg2 and SMs2 both showed decreases with depth, suggesting preferential loss of TN (Figure 2). All cores, except NMg2, exhibited a commonly observed δ^{13}C enrichment with soil depth/age of ~1.5‰ (Figure 2). Among the explanations offered for this pattern is that the enrichment with depth occurs as a combination of the Suess effect (whereby atmospheric CO_2 has become more depleted in ^{13}C in the past century from fossil fuel combustion) and microbial or fungal catabolic reworking of soil carbon resulting in fractionation and increasingly heavier values with greater depth/time (Ehleringer et al., 2000). It has also been observed that relative enrichment of δ^{13}C in roots compared to leaves may contribute to more enriched values with soil depth (Saintilan et al., 2013).

4.2. Potential Mechanisms for Increasing OC Burial

Change in relative SLR is the most likely large-scale driver of increased OC burial rates in the region (Gonneea et al., 2019; Rogers et al., 2019; Watanabe et al., 2019;). Accumulation of the large soil C stocks in this region (Jerath et al., 2016) coincides with late Holocene rates of regional SLR that were largely stable over the past seven millennia, followed by mild acceleration in recent centuries (Gerlach et al., 2017; Khan et al., 2017; Scholl, 1964). Under these conditions, SLR has been a necessary driver of the vertical growth of coastal wetland soils, contributing to the creation of vertical accommodation space for sediment accumulation, enhancement of plant productivity via deposition of nutrients, and ultimately promoting surface elevation increases (Kirwan & Mudd, 2012; Morris et al., 2002; Woodroffe et al., 2016). Similarly, vertical development of soil may respond positively to changes in rates of SLR as rates of productivity and sediment accretion in coastal marshes respond positively and negatively to changes in rates of SLR (Kolker et al., 2009; Morris et al., 1990).

Whereas future work examining the temporal coupling of OC burial rates and relative SLR are necessary to understand the extent and timing of this relationship, gross comparisons of historical sedimentation rates and SLR in the region supply a general explanation of a large-scale driver. The rate of SLR in southwest Florida closely matched rates of mangrove soil accretion in ENP and the RB-NERR region over the periods from 1913 to 2012 and from 1963 to 2012 (Breithaupt et al., 2017). However, from 2003 to 2012, SLR rates exceeded mangrove soil accretion rates by 3 mm year^{-1} (Breithaupt et al., 2017). This discrepancy can be attributed to growing evidence of acceleration in the rate of relative SLR in this region (Park & Sweet, 2015; Wdowinski et al., 2016). Future observations with SETs will tell whether the recent accretion deficit equates to an overall shortfall in vertical development of these soils or whether feedbacks related to soil swelling or root production (Feher et al., 2019; Whelan et al., 2005) increase accordingly.

Evidence of the influence of SLR in the region can be seen in the TN:TP values for core SMs2 (Figure 2). A century ago, this site was extremely P-limited, with TN:TP of ~200, a value almost twice as large as the regional indicator value of mangrove P-limitation of 109 behind Buttonwood Ridge of the southeast Everglades (Castañeda-Moya et al., 2013). In the past century, there has been almost a linear decrease in TN:TP to present-day values of 70, similar to present-day values at SMg1 and SMs1. Although SMs2 has been relatively isolated from allochthonous sediment deposition (Figure 10), the decrease in TN:TP is strong evidence of regional coastal groundwater discharge, which occurs as rising seawater drives the discharge of brackish groundwater (including P) into coastal wetlands (Price et al., 2006).

We propose that SLR can influence OC burial increases in two ways: changes to the quantity of soil OC inputs and changes in OC preservation efficiency. Changes in soil OC inputs may occur as a result of greater allochthonous delivery and/or increased autochthonous production. Evidence of the allochthonous delivery mechanism is supported by increased NC-mineral sediment deposition, which showed significant acceleration in cores SMg1, SMg2, and NMg3 (Figure 10). If the OC would otherwise have been exported from the mangroves to the marine environment (Bouillon et al., 2008; Troxler et al., 2013), then the increase in

burial rates at these sites represents a net increase in the regional carbon sink that was not present a century ago. If the OC is simply being redistributed from one wetland location to another, then OC burial increases at these sites occur at the expense of OC burial decreases and erosion at other sites. However, shifting of previously buried OC due to erosion or resuspension is not a likely driver of the increasing burial rates because such mixing of older and younger soils would disrupt the decay profiles of excess ^{210}Pb seen in the seven cores (Figure 3).

Previous research has shown that hurricane storm surge can be a strong source of nutrient-rich allochthonous sediment (Breithaupt, Hurst, et al., 2019; Castañeda-Moya et al., 2010; Feher et al., 2019; Radabaugh et al., 2019; Whelan et al., 2009) and soil OC (Smoak et al., 2013) for coastlines in this region. These sites demonstrate no significant evidence of Hurricane Wilma (2005) in the ^{210}Pb records, and cores were collected prior to Hurricane Irma (2017) (Figures 5 and 7). However, the MH record at site SMg2 shows an increase in accretion due to sediment deposition during Hurricane Irma (2017) that caused a significant change in the overall trend (Figure 5e) (Whelan et al., 2009). Similar effects were observed at sites along the Shark River and Lostmans River, where sediment deposition due to Hurricane Wilma resulted in immediate elevation gains and multiyear, positive increases in rates of soil elevation change (Feher et al., 2019). Sediment deposition from Irma occurred in the northern region mangrove sites too (Radabaugh et al., 2019) but with substantial spatial variability (indicated by the large error bars after 2017) that did not alter the long-term overall accretion trend of the MH (Figures 5a–5c) or ^{210}Pb data (Figures 7 and 9). The acceleration in OC burial documented by the ^{210}Pb record at site SMg2 (Figure 7) occurred prior to Hurricane Irma. Therefore, while storms contribute substantial pulses of sediment, data from these sites do not support the role of hurricanes as the primary driver of increasing OC burial rates at these sites. Additionally, Radabaugh et al. (2019) observed delayed mangrove mortality 3–9 months after Hurricane Irma in locations near our northern region mangroves, which the authors attributed to smothering by the substantial mud deposits from storm surge. This suggests that short-term gains in carbon burial may be offset by subsequent decreases in soil OC inputs in the absence of root production and litterfall where this delayed mortality occurs. However, mangroves are, in general, highly resilient, disturbance-adapted ecosystems (Krauss & Osland, 2019), and smaller sediment deposits that do not lead to mangrove mortality have the potential to have a positive effect, contributing nutrient-rich sediment inputs that can lead to immediate elevation gains and positive increases in rates of soil elevation change (Feher et al., 2019).

Unsurprisingly, allochthonous NC-mineral sediment deposition was very low and did not show evidence of increase in the marsh cores. Conversely, the basin mangrove site, NMg1, showed a strong negative trend in NC-mineral deposition over the past century (1.73 ± 0.39 g m^{-2} year^{-1}; $p < 0.001$). It is likely the decreasing rates are caused by the core's position behind the fringe berm at the site (Cahoon & Lynch, 1997) and suggests development of the berm in the past century has steadily decreased the amount of allochthonous sediment that reaches the basin. Decreasing rates of allochthonous sediment at this site indicate that increasing OC burial rates must be due to autochthonous processes, most likely related to retention of surface litter behind the berm (Twilley et al., 1986) and elevated porewater salinities of 35–50 within the basin compared to 30 in the surface water (Lynch et al., 1989). This site (NMg1), with decelerating NC-mineral deposition and accelerating OC burial, demonstrates how site-specific characteristics, such as the presence of a berm, contribute to unique patterns of soil composition and accumulation.

Soil OC inputs could also increase if SLR has contributed to enhanced primary production at these locations either in the form of aboveground vegetation, belowground roots, or benthic algal communities. Increased productivity has been shown to occur in salt marshes along a trajectory toward an optimal relationship between water depth, nutrient deposition, and plant productivity (Morris et al., 2002). Increased flooding duration has also been shown to increase mangrove allocation of biomass to belowground components (Castañeda-Moya et al., 2013), a process that could increase soil OC inputs and alter the quality of SOM. Additionally, eutrophication has been shown to increase OC burial rates in an anthropogenically impacted estuary of southeastern Brazil, by increasing the relative contribution of algae to the soil (Sanders et al., 2014). However, data from these sites do not support a similar mechanism for increasing OC burial; while there was some variation in OC:TN in the cores, the consistent depletion of δ^{13}C values from depth to the surface is the opposite of what would occur in the presence of a source-change from mangrove or marsh to algae (Figure 2).

Another possible mechanism for increased OC burial rates in the past century is that OC preservation efficiency has increased. This could occur as a result of two different, not necessarily exclusive, hypotheses: (1) Environmental conditions have changed to be more favorable for the preservation of soil OC, and/or)2) the quality of the OC has changed and become more resistant to degradation. The first hypothesis suggests preservation efficiency may increase with accommodation space and increased depth and duration of flooding, leading to stronger reducing conditions that are less conducive to microbial degradation of soil OC than they were in the past. However, this hypothesis of changing preservation efficiency is not supported by the lignin data (Figures 9 and 11), which show no preferential depth/age of degradation. The second hypothesis proposes that a change in OC quality may occur as the result of changing vegetation type from herbaceous marsh vegetation to woody mangrove vegetation. Attached yellow mangrove leaves and standing sawgrass tissue have similar lignin dry mass content of 10–15% (Benner et al., 1990; Debusk & Reddy, 1998). In contrast, roots have much lower lignin content (Given et al., 1984), in the range of 1.9–2.6% for mangroves in ENP (Poret et al., 2007). As aboveground vegetation falls as litter and interacts with soil, lignin in mangrove leaves may increase to 50% of dry mass (Benner et al., 1990), while the increase for sawgrass is more modest at up to 35% of dry mass (Debusk & Reddy, 1998), suggesting that a change from sawgrass to mangrove litter may manifest as increasing soil lignin content. Evidence of this change may be seen in lignin: OC IFs of 6.7 for SMg1, which has likely exhibited an increase in mangrove presence in the past century, but a largely unchanging lignin: OC IF of 1.1 for SMs1, which has likely been marsh for the past century (Table 2). The observation from this single mangrove-marsh encroachment site at SMg1 suggests that an increase in OC burial rates may accompany a change in vegetation C type.

These mechanisms are not likely to occur exclusively, as there could be interactive effects of increased allochthonous inputs, increased local production, and different burial efficiencies. There also may be negative feedbacks between accommodation space and productivity, whereby increases in productivity lead to greater accretion, which subsequently decreases the accommodation space and limits the deposition of allochthonous sediment (Kirwan & Mudd, 2012). This self-regulating negative feedback will diminish as the rate of SLR outpaces the sediment supply and vegetation productivity that control the soil's vertical growth. These observations suggest that acceleration has occurred in these wetlands because they occupy optimal eco-geomorphic conditions between needing more accommodation space and being drowned by high SLR.

4.3. Blue Carbon Accounting Implications

Although our research focused on mangrove and marsh sites in southwest Florida, these findings have global importance for coastal wetlands in regions experiencing relative SLR. Blue carbon wetlands have amassed large OC soil stocks in many of the tropical and subtropical coastal locations where they are present (Atwood et al., 2017, and references therein, Kauffman & Bhomia, 2017). Recently, long-term OC burial capacity of these blue carbon ecosystems has been tied to global carbon markets (Ullman et al., 2013) and promoted as a conservation and restoration incentive (Sheehan et al., 2019). Thus, it is important to understand the changes in burial rates over time observed here, in order for markets to accurately account carbon credits and ensure that blue carbon restoration targets and financial incentives are realistic (Macreadie et al., 2019).

In the early 1900s, mangroves and coastal freshwater marshes of southwest Florida were burying OC at approximately the same average rate of 28.2 ± 15.0 g m^{-2} year^{-1} (Figure 7). However, over the past ~120 years, OC burial rates have increased by factors ranging from 2.5 to 6.2 for the mangroves and 1.4 to 2.4 for the marshes (Table 2). The result is that the long-term average OC burial rate was 88 ± 13 g m^{-2} year^{-1} for mangroves and 40 ± 10 g m^{-2} year^{-1} for the marshes (Table S2). Without acceleration (i.e., assuming that burial rates would have remained constant throughout the record), soil OC stocks for both wetland types would have increased by 2.82 ± 1.50 kg m^{-2} over the past century. With acceleration, the average soil OC stock has increased by 5.69 ± 0.94 to 8.02 ± 1.73 kg m^{-2} for mangrove forests and 4.16 ± 0.45 to 4.45 ± 0.54 kg m^{-2} for coastal freshwater/brackish marshes (based on the range of IFs; Table 2).

There are 12,435 ha of mangroves and 754 ha of tidal marsh in the RB-NERR (RB-NERR Management Plan 2013). In ENP, there are 144,447 ha of mangroves, with approximately 93,891 ha that are taller than 3 m (Simard et al., 2006). We use the 3 m height to exclude scrub mangroves from southeast ENP, because we have no OC burial rate measurements in scrub mangrove habitat. Based on these areal extents,

acceleration of OC burial in the past century has resulted in soil OC stock increases of 591–1,212 and 27–37 Mg in the mangroves and marshes, respectively, of the RB-NERR and 4,460–9,154 Mg in the mangroves of ENP. We are not aware of an areal estimate for tidal marsh extent in ENP and therefore cannot provide an upscaled estimate for that regional habitat.

In general, we observed that mangrove sites have higher OC and total lignin burial rates than marsh sites in the Everglades (Figures 7 and 8 and Table S2). This difference was discernible for both marsh cores, even though core SMs1 is 270 m closer to the river than SMs2. This suggests there are inherent differences in the factors related to OC burial rates within the two habitat types. The overall higher OC burial rates in mangrove soils means that their encroachment into interior, freshwater marshes has the potential to increase burial rates in those locations more than might be expected from the historical acceleration trends.

5. Conclusion

There is much concern about the potential for SLR to cause degradation and loss of wetland SOM (Hopkinson et al., 2012; Steinmuller et al., 2019), including coastal peat collapse (Chambers et al., 2019) in the coming century. However, these data and our analysis suggest that OC burial in coastal wetlands may be more responsive to SLR than previously thought, including periodic assistance from large storms. We find increasing trends of OC burial in mangrove and coastal marsh soils over the past ~120 years are not an artifact of OC degradation or dating method but represent an acceleration in OC burial. This indicates OC burial rates may not be as stationary as they are normally assumed to be in blue carbon stock assessments. Closer evaluation of fine-scale temporal variability and its causes are needed to better evaluate whether this acceleration represents a net increasing sink or a redistribution of previously buried OC. Finally, these findings do not contradict the cautions raised about the sustainability of these ecosystems in the context of global change. Concluding that OC burial rates have increased over the past century does not alter the fact that SLR is accelerating and will exceed rates experienced by coastal wetlands in the places where they exist today. Increasing OC burial rates will occur only as long as wetland vegetation and soil development can keep pace with accelerating SLR.

Data Availability Statement

Soil core data are available via the Coastal Carbon Research Coordination Network (https://doi.org/10.25573/data.9894266). Marker horizon data are available via the USGS. Northern Region sites: Lynch, J.C., Cahoon, D.R., and Feher, L.C., 2019, Increasing rates of carbon burial in southwest Florida coastal wetlands: U.S. Geological Survey data release (https://doi.org/10.5066/P9ZH3R4G). Southern Region sites: Feher, L.C., Osland, M.J., and Anderson, G.H., 2017, Everglades National Park sediment elevation and marker horizon data release: U.S. Geological Survey data release (https://doi.org/10.5066/F7348HNP).

References

Adair, E. C., Parton, W. J., Del Grosso, S. J., Silver, W. L., Harmon, M. E., Hall, S. A., et al. (2008). Simple three-pool model accurately describes patterns of long-term litter decomposition in diverse climates. *Global Change Biology*, *14*, 2636–2660. https://doi.org/10.1111/j.1365-2486.2008.01674.x

Allison, M. A., Bianchi, T. S., McKee, B. A., & Sampere, T. P. (2007). Carbon burial on river-dominated continental shelves: Impact of historical changes in sediment loading adjacent to the Mississippi River. *Geophysical Research Letters*, *34*, L01606. https://doi.org/10.1029/2006GL028362

Andersen, J. M. (1976). An ignition method for determination of total phosphorus in lake sediments. *Water Research*, *10*, 329–331.

Anderson, G. H., Smith, T. J. III, & Balentine, K. M. (2014). Land-margin ecosystem hydrologic data for the coastal Everglades, Florida, water years 1996–2012: U.S. Geological Survey Data Series. *853*, 38. https://dx.doi.org/10.3133/ds853

Appleby, P. G., & Oldfield, F. (1978). The calculation of Lead-210 dates assuming a constant rate of supply of unsupported 210Pb to the sediment. *Catena*, 5.

Appleby, P.G., & Oldfield, F. (1992). Application of lead-210 to sedimentation studies. In: Ivanovich, M., Harmon, S. (Eds.), *Uranium series disequilibrium: Application to earth, marine and environmental science* (2nd ed., pp. 731-783). Oxford, United Kingdom: Clarendon Press.

Atwood, T. B., Connolly, R. M., Almahasheer, H., Carnell, P. E., Duarte, C. M., Lewis, C. J. E., et al. (2017). Global patterns in mangrove soil carbon stocks and losses. *Nature Climate Change*, *7*(7), 523–528. https://doi.org/10.1038/nclimate3326

Baskaran, M., Bianchi, T. S., & Filley, T. R. (2017). Inconsistencies between 14C and short-lived radionuclide-based sedimentation rates: Effects of long-term mineralization. *Journal of Environmental Radioactivity*, *174*, 10–16.

Benner, R., Weliky, K., & Hedges, J. I. (1990). Early diagenesis of mangrove leaves in a tropical estuary: Molecular-level analyses of neutral sugars and lignin-derived phenols. *Geochimica et Cosmochimica Acta*, *54*, 1991–2001.

Bianchi, T. S., & Canuel, E. A. (2011). *Chemical biomarkers in aquatic ecosystems* (p. 396). Princeton, NJ: Princeton University Press.

Binford, M. W. (1990). Calculation and uncertainty analysis of ^{210}Pb dates for PIRLA project lake sediment cores. *Journal of Paleolimnology*, 253–267.

Bouillon, S., Borges, A. V., Castañeda-Moya, E., Diele, K., Dittmar, T., Duke, N. C., et al. (2008). Mangrove production and carbon sinks: A revision of global budget estimates. *Global Biogeochemical Cycles*, *22*(2), 1–12. https://doi.org/10.1029/2007GB003052

Breithaupt, J. L., Hurst, N., Steinmuller, H. E., Duga, E., Smoak, J. M., Kominoski, J. S., & Chambers, L. G. (2019). Comparing the biogeochemistry of storm surge sediments and pre-storm soils in coastal wetlands: Hurricane Irma and the Florida Everglades. *Estuaries and Coasts*, 1–14. https://doi.org/10.1007/s12237-019-00607-0

Breithaupt, J. L., Smoak, J. M., Byrne, R. H., Waters, M. N., Moyer, R. P., & Sanders, C. J. (2018). Avoiding timescale bias in assessments of coastal wetland vertical change. *Limnology and Oceanography*. https://doi.org/10.1002/lno.10783

Breithaupt, J. L., Smoak, J. M., Rivera-Monroy, V. H., Castañeda-Moya, E., Moyer, R. P., Simard, M., & Sanders, C. J. (2017). Partitioning the relative contributions of organic matter and mineral sediment to accretion rates in carbonate platform mangrove soils. *Marine Geology*, *390*, 170–180. https://doi.org/10.1016/j.margeo.2017.07.002

Breithaupt, J. L., Smoak, J. M., Sanders, C. J., & Troxler, T. G. (2019). Spatial variability of organic carbon, $CaCO_3$ and nutrient burial rates spanning a mangrove productivity gradient in the coastal everglades. *Ecosystems*, *22*(4), 844–858. https://doi.org/10.1007/s10021-018-0306-5

Breithaupt, J. L., Smoak, J. M., Smith, T. J., & Sanders, C. J. (2014). Temporal variability of carbon and nutrient burial, sediment accretion, and mass accumulation over the past century in a carbonate platform mangrove forest of the Florida Everglades. *Journal of Geophysical Research: Biogeosciences*, *119*, 2032–2048. https://doi.org/10.1002/2014JG002715

Breithaupt, J. L., Smoak, J. M., Smith, T. J., Sanders, C. J., & Hoare, A. (2012). Organic carbon burial rates in mangrove sediments: Strengthening the global budget. *Global Biogeochemical Cycles*, *26*(3), 1–11. https://doi.org/10.1029/2012GB004375

Brown, S. A. (1969). Biochemistry of lignin formation. *Bioscience*, *19*, 115–121.

Cahoon, D. R., & Lynch, J. C. (1997). Vertical accretion and shallow subsidence in a mangrove forest of southwestern Florida, USA. *Mangroves and Salt Marshes*, *2100*, 173–186. https://doi.org/10.1023/A:1009904816246

Cahoon, D. R., Lynch, J. C., Hensel, P., Boumans, R. M. J., Perez, B. C., Segura, B., & Day, J. W. (2002). High-precision measurements of wetland sediment elevation: I. Recent improvements to the sedimentation-erosion table. *Journal of Sedimentary Research*, *72*, 730–733.

Cahoon, D. R., Lynch, J. C., Perez, B. C., Segura, B., Holland, R. D., Stelly, C., et al. (2002). High-precision measurements of wetland sediment elevation: II. The rod surface elevation table. *Journal of Sedimentary Research*, *72*, 734–739.

Castañeda-Moya, E., Twilley, R. R., & Rivera-Monroy, V. H. (2013). Allocation of biomass and net primary productivity of mangrove forests along environmental gradients in the Florida Coastal Everglades, USA. *Forest Ecology and Management*, *307*, 226–241. https://doi.org/10.1016/j.foreco.2013.07.011

Castañeda-Moya, E., Twilley, R. R., Rivera-Monroy, V. H., Zhang, K., Davis, S. E., & Ross, M. (2010). Sediment and nutrient deposition associated with Hurricane Wilma in mangroves of the Florida coastal everglades. *Estuaries and Coasts*, *33*(1), 45–58. https://doi.org/10.1007/s12237-009-9242-0

Chambers, L. G., Steinmuller, H. E., & Breithaupt, J. L. (2019). Toward a mechanistic understanding of "peat collapse" and its potential contribution to coastal wetland loss. *Ecology*, *0*(0), 1–15. https://doi.org/10.1002/ecy.2720

Chaopricha, N. A., & Marin-Spiotta, E. (2014). Soil burial contributes to deep soil organic carbon storage. *Soil Biology and Biochemistry*. https://doi.org/10.1016/j.soilbio.2013.11.011

Chmura, G. L., Anisfeld, S. C., Cahoon, D. R., & Lynch, J. C. (2003). Global carbon sequestration in tidal, saline wetland soils. *Global Biogeochemical Cycles*, *17*(4). https://doi.org/10.1029/2002GB001917

Corbett, D. R., Dail, M., & McKee, B. (2007). High-frequency time-series of the dynamic sedimentation processes on the western shelf of the Mississippi River Delta. *Continental Shelf Research*, *27*(10–11), 1600–1615. https://doi.org/10.1016/j.csr.2007.01.025

Corbett, D. R., & Walsh, J. P. (2015). ^{210}Lead and ^{137}Cesium: Establishing a chronology for the last century. In I. Shennan, A. J. Long, & B. P. Horton (Eds.), *Handbook of sea-level research*, (pp. 361–372). John Wiley & Sons, Ltd. https://doi.org/10.1002/9781118452547.ch24

Currie, L. A. (1988). *Detection in analytical chemistry Importance, theory, and practice*. United States: American Chemical Society.

Dean, W. E. (1974). Determination of carbonate and organic matter in calcareous sediments and sedimentary rocks by loss on ignition: Comparison with other methods. *Journal of Sedimentary Research*, *44*(I), 242–248. https://doi.org/10.1306/74D729D2-2B21-11D7-8648000102C1865D

Debusk, W. F., & Reddy, K. R. (1998). Turnover of detrital organic carbon in a nutrient-impacted everglades marsh. *Soil Science Society of America Journal*, *62*, 1460–1468.

DeLaune, R. D., & Reddy, K. R. (2008). *Biogeochemistry of wetlands: Science and applications*. Boca Raton, FL: CRC Press.

Drexler, J. Z., Fuller, C. C., & Arch, S. (2018). The approaching obsolescence of ^{137}Cs dating of wetland soils in North America. *Quaternary Science Reviews*, *199*, 83–96.

Ehleringer, J. T., Buchmann, N., & Flanagan, L. B. (2000). Carbon isotope ratios in belowground carbon cycle processes. *Ecological Applications*, *10*(2), 412–422.

Feher, L. C., Osland, M. J., Anderson, G. H., Vervaeke, W. C., Krauss, K. W., Whelan, K. R. T., et al. (2019). The long-term effects of Hurricanes Wilma and Irma on soil elevation change in Everglades mangrove forests. *Ecosystems*, 1–15. https://doi.org/10.1007/s10021-019-00446-x

FNAI and FWC (Florida Natural Areas Inventory and Florida Fish and Wildlife Conservation Commission). (2016). Cooperative land cover map. http://www.fnai.org/landcover.cfm

Gerlach, M. J., Engelhart, S. E., Kemp, A. C., Moyer, R. P., Smoak, J. M., Bernhardt, C. E., & Cahill, N. (2017). Reconstructing Common Era relative sea-level change on the Gulf Coast of Florida. *Marine Geology*, *390*, 254–269. https://doi.org/10.1016/j.margeo.2017.07.001

Given, P. H., Spackman, W., Painter, P. C., Rhoads, C. A., & Ryan, N. J. (1984). The fate of cellulose and lignin in peats: An exploratory study of the input to coalification. *Organic Geochemistry*, *6*, 399–407.

Gonneea, M. E., Maio, C. V., Kroeger, K. D., Hawkes, A. D., Mora, J., Sullivan, R., et al. (2019). Salt marsh ecosystem restructuring enhances elevation resilience and carbon storage during accelerating relative sea-level rise. *Estuarine, Coastal and Shelf Science*, *217*, 56–68.

Guan, W., Xiong, Y., & Liao, B. (2018). Soil inorganic carbon in mangroves of tropical China: Patterns and implications. *Biology Letters*, *14*. https://doi.org/10.1098/rsbl.2018.0483

Harmon, T. S., Smoak, J. M., Waters, M. N., & Sanders, C. J. (2014). Hydrologic fragmentation-induced eutrophication in Dove Sound, Upper Florida Keys, USA. *Environmental Earth Sciences*, *71*(10), 4387–4395. https://doi.org/10.1007/s12665-013-2832-y

Harris, D., Horwa, W. R., & Van Kessel, C. (2001). Acid fumigation of soils to remove carbonates prior to total organic carbon or Carbon-13 Isotopic Analysis. *Soil Science Society of America Journal*, *65*(6), 1853–1856.

Hedges, J. I., Blanchette, R. A., Weliky, K., & Devol, A. H. (1998). Effects of fungal degradation on the CuO oxidation products of lignin: A controlled laboratory study. *Geochimica et Cosmochimica Acta*, *52*, 2717–2726.

Hedges, J. I., Clark, W. A., & Cowie, G. L. (1988). Organic matter sources to the water column and surficial sediments of a marine bay. *Limnology and Oceanography*, *33*(5), 1116–1136. https://doi.org/10.4319/lo.1988.33.5.1116

Hedges, J. I., & Ertel, J. R. (1982). Characterization of lignin by gas capillary chromatography of cupric oxide oxidation products. *Analytical Chemistry*, *54*, 174–178.

Henrichs, S. M. (1992). Early diagenesis of organic matter in marine sediments: Progress and perplexity. *Marine Chemistry*, *39*(1-3), 119–149.

Hernes, P. J., Robinson, A. C., & Aufdenkampe, A. K. (2007). Fractionation of lignin during leaching and sorption and implications for organic matter "freshness". *Geophysical Research Letters*, *34*, L17401.

Holmquist, J.R., Windham-Myers, L., Bliss, N., Crooks, S., Morris, J.T., Megonigal, J.P., et al. (2018). Accuracy and precision of tidal wetland soil carbon mapping in the Conterminous United States. *Scientific Reports*, (October 2017), 1–16. https://doi.org/10.1038/s41598-018-26948-7

Hopkinson, C. S., Cai, W., & Hu, X. (2012). Carbon sequestration in wetland dominated coastal systems—A global sink of rapidly diminishing magnitude. *Current Opinion in Environmental Sustainability*, *4*, 1–9. https://doi.org/10.1016/j.cosust.2012.03.005

Jenkins, C. (2018). Sediment accumulation rates for the Mississippi delta region: A time-interval synthesis. *Journal of Sedimentary Research*, *88*(February), 301–309.

Jerath, M., Bhat, M., Rivera-Monroy, V. H., Castañeda-Moya, E., Simard, M., & Twilley, R. R. (2016). The role of economic, policy, and ecological factors in estimating the value of carbon stocks in Everglades mangrove forests, South Florida, USA. *Environmental Science and Policy*, *66*, 160–169. https://doi.org/10.1016/j.envsci.2016.09.005

Jex, C. N., Pate, G. H., Blyth, A. J., Spencer, R. G. M., Hernes, P. J., Khan, S. J., & Baker, A. (2014). Lignin biogeochemistry: From modern processes to Quaternary archives. *Quaternary Science Reviews*, *87*, 46–59.

Jiang, J., DeAngelis, D. L., Anderson, G. H., & Smith, T. J. (2013). Analysis and simulation of propagule dispersal and salinity intrusion from storm surge on the movement of a marsh–mangrove ecotone in South Florida. *Estuaries and Coasts*, *37*(1), 24–35. https://doi.org/10.1007/s12237-013-9666-4

Kang, W. J., & Trefry, J. H. (2013). Identifying increased inputs of terrestrial phosphorus to sediments of the southwestern Everglades and Florida Bay. *Estuarine, Coastal and Shelf Science*, *129*, 28–36. https://doi.org/10.1016/j.ecss.2013.06.003

Kauffman, J. B., & Bhomia, R. K. (2017). Ecosystem carbon stocks of mangroves across broad environmental gradients in West-Central Africa: Global and regional comparisons. *PLoS ONE*, *12*(11), 1, e0187749–17. https://doi.org/10.1371/journal.pone.0187749

Khan, N. S., Ashe, E., Horton, B. P., Dutton, A., Kopp, R. E., Brocard, G., et al. (2017). Drivers of Holocene sea-level change in the Caribbean. *Quaternary Science Reviews*, *155*, 13–36. https://doi.org/10.1016/j.quascirev.2016.08.032

Kirwan, M. L., & Mudd, S. M. (2012). Response of salt-marsh carbon accumulation to climate change. *Nature*, *489*(7417), 550–553. https://doi.org/10.1038/nature11440

Kolker, A. S., Goodbred, S. L., Hameed, S., & Cochran, J. K. (2009). High-resolution records of the response of coastal wetland systems to long-term and short-term sea-level variability. *Estuarine, Coastal and Shelf Science*, *84*(4), 493–508. https://doi.org/10.1016/j.ecss.2009.06.030

Krauss, K. W., Demopoulos, A. W. J., Cormier, N., From, A. S., Mcclain-counts, J. P., & Iii, R. R. L. (2018). Ghost forests of Marco Island: Mangrove mortality driven by belowground soil structural shifts during tidal hydrologic alteration. *Estuarine, Coastal and Shelf Science*, *212*(June), 51–62. https://doi.org/10.1016/j.ecss.2018.06.026

Krauss, K. W., & Osland, M. J. (2019). Tropical cyclones and the organization of mangrove forests: A review. *Annals of Botany*. https://doi.org/10.1093/aob/mcz161

Krishnaswamy, S., Lal, D., Martin, J. M., & Meybeck, M. (1971). Geochronology of lake sediments. *Earth and Planetary Science Letters*, *11*, 407e414.

Kuzyakov, Y. (2010). Priming effects: Interactions between living and dead organic matter. *Soil Biology and Biochemistry*, *42*, 1363–1371.

Louchouarn, P., Amon, R. M. W., Duan, S., Pondell, C., Seward, S. M., & White, N. (2010). Analysis of lignin-derived phenols in standard reference materials and ocean dissolved organic matter by gas chromatography/tandem mass spectrometry. *Marine Chemistry*, *118*, 85–97.

Lynch, J.C., Hensel, P. & Cahoon, D.R. (2015) The surface elevation table and marker horizon technique: A protocol for monitoring wetland elevation dynamics. Natural Resources Report NPS/NCBN/NRR-2015/1078. U.S. National Park Service, Fort Collins, Colorado, USA.

Lynch, J. C., Meriwether, J. R., McKee, B. A., Vera-Herrera, F., & Twilley, R. R. (1989). Recent accretion in mangrove ecosystems based on ^{137}Cs and ^{210}Pb. *Estuaries*, *12*, 284–299. https://doi.org/10.2307/1351907

MacKenzie, A. B., Hardie, S. M. L., Farmer, J. G., Eades, L. J., & Pulford, I. D. (2011). Analytical and sampling constraints in ^{210}Pb dating. *Science of the Total Environment*, *409*(7), 1298–1304. https://doi.org/10.1016/j.scitotenv.2010.11.040

Macreadie, P. I., Anton, A., Raven, J. A., Beaumont, N., Connolly, R. M., Friess, D. A., et al. (2019). The future of blue carbon science. *Nature Communications*, *10*(1), 1–13. https://doi.org/10.1038/s41467-019-11693-w

Marchio, D., Savarese, M., Bovard, B., & Mitsch, W. (2016). Carbon sequestration and sedimentation in mangrove swamps influenced by hydrogeomorphic conditions and urbanization in Southwest Florida. *Forests*, *7*(6), 116. https://doi.org/10.3390/f7060116

Marin-Spiotta, E., Chaopricha, N. T., Plante, A. F., Diefendorf, A. F., Mueller, C. A., Grandy, A. S., & Mason, J. A. (2014). Long-term stabilization of deep soil carbon by fire and burial during early Holocene climate change. *Nature Geoscience*, *1*(6), 341. https://doi.org/10.1038/NGEO216

Mcleod, E., Chmura, G. L., Bouillon, S., Salm, R., Björk, M., Duarte, C. M., et al. (2011). A blueprint for blue carbon: Toward an improved understanding of the role of vegetated coastal habitats in sequestering $CO2$. *Frontiers in Ecology and the Environment*, *9*(10), 552–560. https://doi.org/10.1890/110004

Moreira-Vilar, F. C., de Cassia Siqueira-Soares, R., Finger-Teixeira, A., de Oliveira, D. M., Ferro, A. P., da Rocha, G. J., et al. (2014). The acetyl bromide method is faster, simpler and presents best recovery of lignin in different herbaceous tissues than Klason and thioglycolic acid methods. *PLoS ONE*, *9*(10), e110000. https://doi.org/10.1371/journal.pone.0110000

Morris, J. T., Kjerfve, B., & Dean, J. M. (1990). Dependence of estuarine productivity on anomalies in mean sea level. *Limnology and Oceanography*, *35*(4), 926–930.

Morris, J. T., Sundareshwar, P. V., Nietch, C. T., Kjerfve, B., & Cahoon, D. R. (2002). Responses of coastal wetlands to rising sea level. *Ecology*, *83*(10), 2869–2877.

Nolte, S., Koppenaal, E. C., Esselink, P., Dijkema, K. S., Schuerch, M., De Groot, A. V., et al. (2013). Measuring sedimentation in tidal marshes: A review on methods and their applicability in biogeomorphological studies. *Journal of Coastal Conservation*, *17*(3), 301–325. https://doi.org/10.1007/s11852-013-0238-3

Opsahl, S., & Benner, R. (1995). Early diagenesis of vascular plant tissues: Lignin and cutin decomposition and biogeochemical implications. *Geochimica et Cosmochimica Acta*, *59*, 4889–4904.

Otto, A., & Simpson, M. (2006). Evaluation of CuO oxidation parameters for determining the source and stage of lignin degradation in soil. *Biogeochemistry*, *80*, 121–142.

Ouyang, X., & Lee, S. Y. (2014). Updated estimates of carbon accumulation rates in coastal marsh sediments. *Biogeosciences*, *11*(18), 5057–5071. https://doi.org/10.5194/bg-11-5057-2014

Park, J., & Sweet, W. (2015). Accelerated sea level rise and Florida Current transport. *Ocean Science*, *11*(4), 607–615. https://doi.org/10.5194/os-11-607-2015

Parkinson, R., DeLaune, R., & White, J. (1994). Holocene sea-level rise and the fate of mangrove forests within the wider Caribbean region. *Journal of Coastal Research*, *10*(4), 1077–1086.

Parkinson, R. W., Craft, C., DeLaune, R. D., Donoghue, J. F., Kearney, M., Meeder, J. F., et al. (2017). Marsh vulnerability to sea-level rise. *Nature Climate Change*, *7*(November), 756.

Poret, N., Twilley, R. R., Rivera-Monroy, V. H., & Coronado-Molina, C. (2007). Belowground decomposition of mangrove roots in Florida coastal everglades. *Estuaries and Coasts*, *30*(3), 491–496. https://doi.org/10.1007/BF02819395

Price, R. M., Swart, P. K., & Fourqurean, J. W. (2006). Coastal groundwater discharge—An additional source of phosphorus for the oligotrophic wetlands of the Everglades. *Hydrobiologia*, *569*(1), 23–36. https://doi.org/10.1007/s10750-006-0120-5

Radabaugh, K. R., Moyer, R. P., Chappel, A. R., Dontis, E. E., Russo, C. E., Joyse, K. M., et al. (2019). Mangrove damage, delayed mortality, and early recovery following Hurricane Irma at two landfall sites in southwest Florida, USA. *Estuaries and Coasts*, 1–15. https://doi.org/10.1007/s12237-019-00564-8

Rogers, K., Kelleway, J. J., Saintilan, N., Megonigal, J. P., Adams, J. B., Holmquist, J. R., et al. (2019). Wetland carbon storage controlled by millennial-scale variation in relative sea-level rise. *Nature*, *567*(7746), 91–95. https://doi.org/10.1038/s41586-019-0951-7

RB-NERR: Rookery Bay National Estuarine Research Reserve Management Plan January 2012 – December 2017. https://coast.noaa.gov/data/docs/nerrs/Reserves_RKB_MgmtPlan.pdf

Saha, A. K., Moses, C. S., Price, R. M., Engel, V., & Smith, T. J. III (2012). A hydrological budget (2002–2008) for a large subtropical wetland ecosystem indicates marine groundwater discharge accompanies diminished freshwater flow. *Estuaries and Coasts*, *35*, 459–474. https://doi.org/10.1007/s12237-011-9454-y

Saintilan, N., Rogers, K., Mazumder, D., & Woodroffe, C. (2013). Allochthonous and autochthonous contributions to carbon accumulation and carbon store in southeastern Australian coastal wetlands. *Estuarine, Coastal and Shelf Science*, *128*, 1–9. https://doi.org/10.1016/j.ecss.2013.05.010

Sanders, C. J., Eyre, B. D., Santos, I. R., Machado, W., Luiz-Silva, W., Smoak, J. M., et al. (2014). Elevated rates of organic carbon, nitrogen and phosphorus accumulation in a highly impacted mangrove wetland. *Geophysical Research Letters*, 1–6. https://doi.org/10.1002/2014GL059789

Scholl, D. (1964). Recent sedimentary record in mangrove swamps and rise in sea level over the southwestern coast of Florida: Part 1. *Marine Geology*, *1*, 344–366.

Schropp, S. J., Graham Lewis, F., Windom, H. L., Ryan, J. D., Calder, F. D., & Burney, L. C. (1990). Interpretation of metal concentrations in estuarine sediments of Florida using aluminum as a reference element. *Estuaries*, *13*(3), 227.

Sheehan, L., Sherwood, E. T., Moyer, R. P., Radabaugh, K. R., Simpson, S., & Simpson, S. (2019). Blue carbon: An additional driver for restoring and preserving ecological services of coastal wetlands in Tampa Bay their ability to sequester and store disproportionately large. *Wetlands*, *2*, 1–12. https://doi.org/https://doi.org/10.1007/s13157-019-01137-y

Shields, M. R., Bianchi, T. S., Kolker, A. S., Kenney, W. F., Mohrig, D., Osborne, T. Z., & Curtis, J. H. (2019). Factors controlling storage, sources, and diagenetic state of organic carbon in a prograding subaerial delta: Wax Lake Delta, Lousiana. *Journal of Geophysical Research – Biogeosciences*, *124*, 1115–1131. https://doi.org/10129/2019JG004683

Shields, M. R., Bianchi, T. S., Mohrig, D., Kenney, W. H., Kolker, A. S., & Curtis, J. S. (2017). Ecosystem engineering builds coastline and stores blue carbon in the Mississippi River Delta Complex. *Nature Geoscience*, *10*, 846–851.

Simard, M., Zhang, K., Rivera-Monroy, V. H., Ross, M. S., Ruiz, P. L., Castañeda-Moya, E., et al. (2006). Mapping height and biomass of mangrove forests in Everglades National Park with SRTM elevation data. *Photogrammetric Engineering & Remote Sensing*, *72*(3), 299–311.

Smith, T. J., Anderson, G. H., Balentine, K., Tiling, G., Ward, G. A., & Whelan, K. R. T. (2009). Cumulative impacts of hurricanes on Florida mangrove ecosystems: Sediment deposition, storm surges and vegetation. *Wetlands*, *29*(1), 24–34. https://doi.org/10.1672/08-40.1

Smith, T. J., Foster, A. M., Tiling-Range, G., & Jones, J. W. (2013). Dynamics of mangrove-marsh ecotones in subtropical coastal wetlands: Fire, sea-level rise, and water levels. *Fire Ecology*, *9*(1), 66–77. https://doi.org/10.4996/fireecology.0901066

Smoak, J., Breithaupt, J., Smith, T. III, & Sanders, C. (2013). Sediment accretion and organic carbon burial relative to sea-level rise and storm events in two mangrove forests in Everglades National Park. *Catena*, *104*, 58–66. https://doi.org/DOI, https://doi.org/10.1016/j.catena.2012.10.009

Steinmuller, H. E., Dittmer, K. M., White, J. R., & Chambers, L. G. (2019). Understanding the fate of soil organic matter in submerging coastal wetland soils: A microcosm approach. *Geoderma*, *337*(December 2017), 1267–1277. https://doi.org/10.1016/j.geoderma.2018.08.020

Thevenot, M., Dignac, M.-F., & Rumpel, C. (2010). Fate of lignins in soils: A review. *Soil Biology and Biochemistry*, *42*, 1200–1211.

Troxler, T. G., Gaiser, E., Barr, J., Fuentes, J. D., Jaffe, R., Childers, D. L., et al. (2013). Integrated carbon budget models for the Everglades terrestrial-coastal-oceanic gradient: Current status and needs for inter-site comparisons. *Oceanography*, *26*(3), 98–107.

Twilley, R. W., Lugo, A. E., & Patterson-Zucca, C. (1986). Litter production and turnover in basin mangrove forests in Southwest Florida. *Ecology*, *67*(3), 670–683.

Ullman, R., Bilbao-Bastida, V., & Grimsditch, G. (2013). Including blue carbon in climate market mechanisms. *Ocean and Coastal Management*, *83*, 15–18.

Watanabe, K., Seike, K., Kajihara, R., Montani, S., & Kuwae, T. (2019). Relative sea-level change regulates organic carbon accumulation in coastal habitats. *Global Change Biology*, 1–15. https://doi.org/10.1111/gcb.14558

Wdowinski, S., Bray, R., Kirtman, B. P., & Wu, Z. (2016). Increasing flooding hazard in coastal communities due to rising sea level: Case study of Miami Beach, Florida. *Ocean and Coastal Management*, *126*, 1–8. https://doi.org/10.1016/j.ocecoaman.2016.03.002

Weston, N. B. (2014). Declining sediments and rising seas: An unfortunate convergence for tidal wetlands. *Estuaries and Coasts*, *37*, 1–23. https://doi.org/10.1007/s12237-013-9654-8

Whelan, K. R. T., Smith, T. J. III, Anderson, G. H., & Ouellette, M. L. (2009). Hurricane Wilma's impact on overall soil elevation and zones within the soil profile in a mangrove forest. *Wetlands*, *29*, 16–23.

Whelan, K. R. T., Smith, T. J. III, Cahoon, D. R., Lynch, J. C., & Anderson, G. H. (2005). Groundwater control of mangrove surface elevation: Shrink and swell varies with soil depth. *Estuaries and Coasts*, *28*, 833–843.

Woodroffe, C. D., Rogers, K., McKee, K. L., Lovelock, C. E., Mendelssohn, I. A., & Saintilan, N. (2016). Mangrove sedimentation and response to relative sea-level rise. *Annual Review of Marine Science*, *8*(1), 243–266.

Zimmerman, A. R., & Canuel, E. A. (2000). A geochemical record of eutrophication and anoxia in Chesapeake Bay sediments: Anthropogenic influence on organic matter composition. *Marine Chemistry*, *69*, 117–137.